



HAL
open science

Deep crustal source of gneiss dome revealed by eclogite in migmatite (Montagne Noire, French Massif Central)

Donna L. Whitney, Clementine Hamelin, Christian Teyssier, Natalie Raia, Megan Korchinski, Nicholas Seaton, Brian Bagley, Anette Handt, Françoise Roger, Patrice Rey

► To cite this version:

Donna L. Whitney, Clementine Hamelin, Christian Teyssier, Natalie Raia, Megan Korchinski, et al.. Deep crustal source of gneiss dome revealed by eclogite in migmatite (Montagne Noire, French Massif Central). *Journal of Metamorphic Geology*, 2020, 38 (3), pp.297-327. 10.1111/jmg.12523 . hal-02510842

HAL Id: hal-02510842

<https://hal.umontpellier.fr/hal-02510842>

Submitted on 29 Oct 2020

HAL is a multi-disciplinary open access archive for the deposit and dissemination of scientific research documents, whether they are published or not. The documents may come from teaching and research institutions in France or abroad, or from public or private research centers.

L'archive ouverte pluridisciplinaire **HAL**, est destinée au dépôt et à la diffusion de documents scientifiques de niveau recherche, publiés ou non, émanant des établissements d'enseignement et de recherche français ou étrangers, des laboratoires publics ou privés.

Deep crustal source of gneiss dome revealed by eclogite in migmatite (Montagne Noire, French Massif Central)

*Donna L. Whitney**, *Clémentine Hamelin*, *Christian Teyssier*, *Natalie H. Raia*, *Megan S. Korchinski*,
Nicholas C.A. Seaton, *Brian C. Bagley*, *Anette von der Handt*

Department of Earth Sciences, University of Minnesota, Minneapolis MN 55455 USA

Françoise Roger

Laboratoire Géosciences Montpellier (CNRS-UMR 5243), Université Montpellier, 34095 Montpellier
Cedex 5, France

Patrice F. Rey

School of Geosciences, University of Sydney, Sydney, NSW 2006, Australia

* corresponding author (email: dwhitney@umn.edu)

Short running title: Deep crustal source of gneiss dome

This article has been accepted for publication and undergone full peer review but has not been through the copyediting, typesetting, pagination and proofreading process, which may lead to differences between this version and the [Version of Record](#). Please cite this article as [doi: 10.1111/JMG.12523](https://doi.org/10.1111/JMG.12523)

This article is protected by copyright. All rights reserved

ABSTRACT

In orogens worldwide and throughout geologic time, large volumes of deep continental crust have been exhumed in domal structures. Extension-driven ascent of bodies of deep, hot crust is a very efficient mechanism for rapid heat and mass transfer from deep to shallow crustal levels and is therefore an important mechanism in the evolution of continents. The dominant rock type in exhumed domes is quartzofeldspathic gneiss (typically migmatitic) that does not record its former high-pressure (HP) conditions in its equilibrium mineral assemblage; rather, it records the conditions of emplacement and cooling in the mid/shallow crust. Mafic rocks included in gneiss may, however, contain a fragmentary record of a HP history and are evidence that their host rocks were also deeply sourced.

An excellent example of exhumed deep crust that retains a partial HP record is in the Montagne Noire dome, French Massif Central, which contains well-preserved eclogite (garnet + omphacite + rutile + quartz) in migmatite in two locations: one in the dome core and the other at the dome margin. Both eclogites record $P \sim 1.5 \pm 0.2$ GPa at $T \sim 700 \pm 20^\circ\text{C}$, but differ from each other in whole-rock and mineral composition, deformation features (shape and crystallographic preferred orientation), extent of record of prograde metamorphism in garnet and zircon, and degree of preservation of inherited zircon. Rim ages of zircon in both eclogites overlap with the oldest crystallization ages of host gneiss at $c. 310$ Ma, interpreted based on zircon REE abundance in eclogite zircon as the age of HP metamorphism. Dome-margin eclogite zircon retains a widespread record of protolith age ($c. 470$ - 450 Ma, the same as host gneiss protolith age), whereas dome-core eclogite zircon has more scarce preservation of inherited zircon. Possible explanations for differences in the two eclogites relate to differences in the protolith mafic magma composition and history and/or the duration of metamorphic heating and extent of interaction with aqueous fluid, affecting zircon crystallization. Differences in HP deformation fabrics may relate to position of the eclogite-facies rocks relative to zones of transpression and transtension at an early stage of dome development. Regardless of differences, both eclogites experienced HP metamorphism and deformation in the deep crust at $c. 310$ Ma and were exhumed by lithospheric extension – with their host migmatite – near the end of the Variscan orogeny. The deep crust in this region was rapidly exhumed from ~ 50 km to <10 km, where it equilibrated under low- P / high- T conditions, leaving a sparse but compelling record of the deep

origin of most of the crust now exposed in the dome.

KEYWORDS

deep crust, eclogite, gneiss dome, migmatite, Montagne Noire

Accepted Article

1. INTRODUCTION

Eclogite- and high-pressure (HP) granulite-facies rocks hosted by quartzofeldspathic gneiss occur in continental orogens such as the European Variscides (e.g. Cabanis & Godard, 1987; O'Brien & Carswell, 1993; Demange, 1985; Stipska, Schulmann, & Powell, 2008; Gaggero, Buzzi, Haydoutov, & Cortesogno, 2009) and the Himalayas (Groppo, Lombardo, Rolfo, & Pertusati, 2007; Cottle, Jessup, Newell, Horstwood, Noble, Parrish, Waters, & Searle, 2009; Corrie, Kohn, & Vervoort, 2010), including ultrahigh-pressure (UHP) terrains such as the Western Gneiss Region, Norway (Wain, 1997; Cuthbert, Carswell, Krogh Ravna, & Wain, 2000), the Woodlark Rift, Papua New Guinea (Hill & Baldwin, 1993; Baldwin, Webb, & Monteleone, 2008; Little, Hacker, Gordon, Baldwin, Fitzgerald, Ellis, & Korchinski, 2011) and the Dabie-Sulu and Qaidam regions, China (Okay, 1993; Zhao, Zheng, Chen, Xia, & Wu, 2007; Mattinson, Wooden, Liou, Bird, & Wu, 2006). Host gneiss typically does not record (U)HP conditions, leading to longstanding controversy about the relationship of eclogite inclusions and host gneiss (Eskola, 1921; Lappin & Smith, 1978; Brueckner, 2018). In orogens and continental subduction terrains, geochronology results for eclogite and enclosing gneiss may be the same or similar (e.g. Carswell, Brueckner, Cuthbert, Mehta, & O'Brien, 2003; Yang, Wooden, Wu, Liu, Xu, Shi, Katayama, Liou, & Maruyama, 2003; Gordon, Whitney, Teyssier, & Fossen, 2013), raising questions about pressure-temperature-time histories of inclusions and host. There is increasing recognition that gneiss and mafic (U)HP inclusions shared much of their metamorphic history (e.g. Stipska *et al.*, 2008; Gordon *et al.*, 2013; Whitney, Roger, Teyssier, Rey, & Respaut, 2015). In such cases, the pressure-temperature-time-deformation (P - T - t - d) history of mafic and other refractory inclusions may provide information that has been obliterated in the quartzofeldspathic host rocks.

In orogenic and continental subduction settings, gneiss that hosts (U)HP layers and lenses commonly comprises domal structures (i.e., domes of foliation) that formed during exhumation (Teyssier & Whitney, 2002; Whitney, Teyssier, & Vanderhaeghe, 2004; Labrousse, Prouteau, & Ganzhorn, 2011). An excellent example of HP rocks exhumed in a gneiss (migmatite) dome is the Montagne Noire dome of the Variscan Massif Central, France (Fig. 1a), as this dome contains relics of HP mafic and pelitic rocks. Relict kyanite has been observed in paragneiss that records in its dominant matrix assemblage a later, lower- P history (Bouchardon, Déchomets, & Demange 1979;

Fréville, Cenki-Tok, Trap, Rabin, Leyreloup, Regnier, & Whitney, 2016), and some mafic rocks preserve an early HP (eclogite-facies) history (Demange, 1985) (Fig. 1b). Two localities in the dome contain well-preserved (garnet + omphacite-bearing) eclogite lenses in gneiss: one in the core of the dome (Terme de Fourcaric - Peyrambert) and the other at the margin (Cabardès) (Fig. 1b). The P - T - t history of eclogites at these two sites is the focus of this paper.

In this paper, we present new results for P - T conditions, timing of metamorphism, and deformation histories of eclogite from the Montagne Noire dome-core and dome-margin and use these to track the magnitude and trajectory of deep crustal flow. We use thermobarometric methods for estimation of P - T conditions (e.g. Zr-in-rutile and Ti-in-zircon thermometry, bulk-composition-specific phase diagrams), geochronology (U-Pb dating of zircon in eclogite), geochemistry (whole-rock and zircon trace-element composition), and structural analysis (electron back-scattered diffraction analysis of omphacite crystallographic preferred orientation, X-ray computed tomography imaging of rutile shape fabrics). These results are integrated in a discussion of the metamorphism and deformation of the eclogites and their significance for recognizing the extent and mechanisms of exhumation of the deep-crust in orogens.

2. PETROLOGY AND STRUCTURE OF THE MONTAGNE NOIRE DOME

The Montagne Noire, at the southern margin of the French Massif Central (Fig. 1a), is an elongate domal structure that consists primarily of gneissic rocks and crustally-derived granite (e.g. Géze, 1949; Schuiling, 1960; Bouchardon *et al.*, 1979; Demange, Guérangé-Lozes, & Guérangé, 1996; Aerden, 1998). The gneissic core is comprised of two major subdomes – the Espinouse-Laouzas (north) and Caroux-Somail-Nore (south) domes – that flank a steep high-strain zone (Rey *et al.*, 2011; Rabin *et al.*, 2015) (Fig. 1b). Cordierite occurs in gneiss and granite, as well as in schist in the carapace of the dome (Thompson & Bard, 1982; Fréville *et al.*, 2016). The presence of cordierite and andalusite in the schist carapace indicates the low- P / high- T metamorphic conditions associated with the latter stages of dome emplacement, following earlier higher- P metamorphism as indicated by the relict kyanite in the dome and the schist carapace (Bouchardon *et al.*, 1979; Demange, 1985; Fréville *et al.*, 2016) (Fig. 1b). The dome also contains metamorphosed mafic and ultramafic layers and pods,

with rare eclogite-facies assemblages preserved in metabasaltic rocks (Demange, 1985; Faure, Cocherie, Gaché, Esnault, Guerrot, Rossi, Wei, & Qiuli, 2014; Whitney *et al.*, 2015).

Protoliths of the gneiss have been dated by U-Pb zircon analysis at *c.* 520 Ma and *c.* 470-450 Ma (Ducrot, Lancelot, & Marchand, 1983; Roger, Respaut, Brunel, Matte, & Paquette, 2004; Cocherie, Baudin, Autran, Guerrot, Fanning, & Laumonier, 2005; Pitra, Poujol, van den Driessche, Poilvet, & Paquette 2012; Roger, Teyssier, Respaut, Rey, Jolivet, Whitney, Paquette, Brunel, & Matte, 2015; Trap, Roger, Cenki-Tok & Paquette, 2017). High-*T* metamorphism and deformation of gneiss/schist has been determined by U-Th-Pb monazite ages at *c.* 315-300 Ma (Roger *et al.*, 2015; Trap, Roger, Cenki-Tok, & Paquette, 2017) and by U-Pb zircon dating of a syntectonic felsic dike at *c.* 309 Ma (Franke, Doublier, Klama, Potel, & Wemmer, 2011).

2.1 Eclogites in the Montagne Noire dome

Eclogite-facies mafic rocks in the Montagne Noire dome occur within migmatitic orthogneiss and paragneiss as boudinaged layers ranging in length from meters to tens of meters. Mafic rocks in the dome are significantly more abundant as amphibolite, which has a whole-rock composition that is very similar to the composition of the eclogite (Demange, 1985).

There are three localities in which eclogite with mafic protoliths is at least partially preserved. Two are in the dome core (Terme de Fourcaric–Peyrambert, Le Jounié) and one is at the dome margin (Cabardès) (Fig. 1b). The Terme de Fourcaric (dome core) and Cabardès (dome margin) localities contain the assemblage garnet + omphacite + rutile ± quartz (Table 1). At the other dome-core locality (Le Jounié), garnet is partially preserved, typically with extensive replacement of the rim by amphibole-pyroxene-plagioclase symplectite. Omphacite, however, is entirely pseudomorphed by amphibole-pyroxene-plagioclase symplectite, and rutile has been partially replaced by ilmenite or titanite. Other reported localities (Demange, 1985; Alabouvette, Demange, Guérangé-Lozes, & Ambert, 2003) are metamorphosed ultramafic rocks, including peridotite and inferred cumulate gabbro, or are extensively retrogressed in the amphibolite or greenschist facies. For example, the Gorge d'Heric/Airette locality (Fig. 1b) has been interpreted as an eclogite-facies gabbro cumulate (Demange, 1985); it contains diopside, enstatite, garnet, and olivine – but no omphacite – and has abundant texturally-late amphibole.

The Terme de Fourcaric-Peyrebert eclogite – hereafter referred to as the Terme de Fourcaric or dome-core eclogite – contains garnet with distinct core and rim as defined by compositional zoning and inclusions: almandine-rich, quartz-inclusion-bearing garnet cores record prograde amphibolite-facies metamorphism, whereas pyrope-rich garnet rims that contain rutile inclusions record eclogite-facies metamorphism (Whitney *et al.*, 2015). Peak *P-T* conditions for the assemblage garnet (rim) + omphacite + rutile + quartz (minor) were determined by a combination of bulk-composition-specific phase diagram modeling, Zr-in-rutile thermometry, and Grt-Cpx thermometry at $\sim 725^{\circ}\text{C}$, 1.4 GPa. Peak conditions were followed by decompression and partial retrogression, as recorded by the presence of symplectitic amphibole + pyroxene + plagioclase \pm biotite replacement of garnet and omphacite, and by ilmenite/titanite rims on rutile (Whitney *et al.*, 2015).

Previous geochronology studies of dome-core eclogite used LA-ICPMS, SHRIMP, and/or SIMS and obtained U-Pb ages of *c.* 315-308 Ma (zircon rims, most zircon cores, rutile) (Peyrebert: Faure *et al.*, 2014; Terme de Fourcaric: Whitney *et al.*, 2015). These studies also determined ages of *c.* 360-365 Ma from U-Pb LA-ICPMS analysis of some zircon cores (Whitney *et al.*, 2015) and from the Sm-Nd isochron method using resorbed garnet + whole-rock + pyroxene (Faure *et al.*, 2014), although the two studies differed in their interpretation of these ages. Faure *et al.* (2014) proposed that eclogite metamorphism occurred at *c.* 360 Ma, with a later (*c.* 315 Ma) hydrothermal metamorphism that produced zircon and rutile. Whitney *et al.* (2015) used zircon rare-earth element (REE) data indicating that the *c.* 315 Ma age corresponded to crystallization of zircon with garnet to interpret this as the age of *HP* metamorphism. REE trends indicate that the *c.* 360 Ma age corresponded to crystallization with plagioclase, so this age was interpreted as the timing of an amphibolite-facies event that corresponded to the growth of garnet cores. In contrast, the Cabardès (dome-margin) eclogite was previously determined to be significantly older than the dome-core eclogite: in a U-Pb zircon study (ID-TIMS), Gebauer & Grünenfelder (1982) obtained a lower-intercept age of 432 Ma. We provide here the first geochronology results for individual zircon crystals in the dome-margin eclogite and show that this eclogite is the same age as the dome-core eclogite.

In this paper, we focus on the Terme de Fourcaric dome-core and the Cabardès dome-margin eclogite localities because they contain garnet and omphacite, although we also provide whole-rock geochemical data for the retrogressed (no preserved omphacite) dome-core Le Jounié eclogite for

comparison. We document the metamorphic petrology (including P - T conditions) and age of the Cabardès eclogite, and integrate these data with previously-published (Whitney *et al.*, 2015) and new results from the Terme de Fourcaric eclogite.

3. METHODS

3.1 Whole-rock major and trace element analyses (XRF, ICP-MS)

In order to understand the prototectonic setting of the mafic protoliths and to characterize bulk-rock composition for use in calculation of phase diagrams, we determined the whole-rock major and trace element (including REE) composition of the freshest eclogite (preserved garnet + omphacite) as well as partially retrogressed eclogite (Fig. 2; Table 1). Whole-rock analyses of 11 eclogite samples (6 dome-core, 5 dome-margin) were conducted at the Washington State University GeoAnalytical Lab. Major elements were prepared and analyzed on a ThermoARL Advant'XP+ sequential X-ray fluorescence (XRF) spectrometer using the method of Johnson, Hooper, & Conrey (1999). Trace elements were prepared and analyzed on an Agilent quadrupole ICP-MS.

3.2 Mineral major and trace element analyses (electron probe microanalysis, EPMA)

Mineral compositions were determined from dome-margin eclogite using a JEOL JXA-8530FPlus electron microprobe in the Department of Earth & Environmental Sciences at the University of Minnesota. The JXA-8530FPlus has four wavelength-dispersive spectrometers. Analytical conditions included a 15-kV accelerating voltage and a 15 nA beam current for all minerals except rutile. Rutile was analyzed with a 20-kV accelerating voltage and a beam current of 100 nA. The beam was focused ($<1\ \mu\text{m}$) for analysis of garnet, clinopyroxene, and rutile. Natural mineral standards were used in calibrations, and the CITZAF matrix correction (Armstrong, 1988) was applied for major phases; details of the rutile analytical protocol are in Whitney *et al.* (2015), where mineral compositions for the dome-core eclogite are also presented. X-ray element maps (Fe, Mn, Mg, Ca) were acquired using a 100 nA beam current and a focused beam, and trace element maps (Cr, P, Sc, Y) were acquired using a 700 nA current and a $3\ \mu\text{m}$ beam diameter.

3.3 Geochronology: U-Pb dating (SHRIMP, LA-ICPMS)

Zircon U-Pb ages were determined for two eclogite samples – one from the dome-margin and one from the dome-core – using the Sensitive High-Resolution Ion Microprobe (SHRIMP II) at the Research School of Earth Sciences at the Australian National University (ANU). A dome-core eclogite sample was previously dated by the LA-ICPMS U-Th-Pb technique in the Laboratoire Magmas et Volcans, Clermont Ferrand, France (Whitney *et al.*, 2015). A sample from the same dome-core eclogite was analyzed on the SHRIMP II for direct comparison of results from the dome-margin eclogite.

For SHRIMP analyses, zircon from the dome-margin eclogite was separated at the University of Minnesota using conventional magnetic separation and heavy liquids methods. Zircon grains were handpicked at the ANU, placed onto double-sided tape, mounted in epoxy together with chips of TEMORA 2 reference zircon (Black, Kamo, Allen, Aleinikoff, Davis, Korsch, R.J., & Foudoulis 2003), and polished down approximately to equatorial mid-section. Reflected and transmitted light photomicrographs were prepared for all zircons, as were cathodoluminescence (CL) Scanning Electron Microscope images. The CL images were used to decipher the internal structure of the sectioned grains and to evaluate whether the $\sim 10\ \mu\text{m}$ spot size was wholly within a single zoning domain. Instrumental conditions and data acquisition on SHRIMP II followed that of Williams (1998). Each analysis consisted of 6 scans through the mass range, with a TEMORA 2 reference zircon analyzed for every three unknown analyses. The data were reduced using the SQUID Excel Macro of Ludwig (2001). U/Pb ratios were normalized relative to a value of 0.0668 for the TEMORA reference zircon, equivalent to a TIMS age of 417 Ma (Black *et al.*, 2003). Data were corrected for common lead using the measured $^{238}\text{Pb}/^{206}\text{Pb}$ and $^{207}\text{Pb}/^{206}\text{Pb}$ ratios following Tera & Wasserburg (1972) as outlined in Williams (1998). Uncertainty in the U-Pb calibration was 0.49% and 0.37% for the respective SHRIMP II sessions. This uncertainty has been added in quadrature, following the weighted mean age calculations. Weighted mean $^{206}\text{Pb}/^{238}\text{U}$ age calculations, reported with 95% confidence limits, were carried out using ISOPLOT/EX (Ludwig, 2003).

Zircon grains from the dome-margin eclogite were also analyzed using LA-ICPMS at the University of California, Santa Barbara, in order to obtain U-Pb age data and REE abundances simultaneously from the same volume of ablated material (Kylander-Clark, Hacker, & Cottle, 2013). Owing to the thinness of metamorphic rim zones, zircon grains were depth-profiled using laser

ablation split-stream (LASS)-ICPMS, from the outer surface of the zircon grains into the interior of the grains. Rims range in thickness from a fraction of a micrometer (μm) to tens of μm . In most cases, these domains are too narrow to analyze using a conventional laser ablation spot of $\sim 15 \mu\text{m}$ in diameter, and this can lead to apparent older ages from mixing with adjacent or underlying core domains.

Nine zircon grains were selected from separates used for SHRIMP analyses, mounted on ultra-flat Kapton tape, embedded in epoxy, and left unpolished. All nine grains were analyzed using a Photon Machines Analyte 193nm Excimer Laser with HelEx ablation cell, combined with a Nu Instruments HR plasma high-resolution multi-collector ICP-MS for U-Th-Pb data collection, and an Agilent 7700S quadrupole ICP-MS for REE, major and trace element data collection. The instrument was operated with energy settings of 4 mJ, repetition rate of 2Hz with a laser fluence of $\sim 1.5 \text{ J}\cdot\text{cm}^{-2}$, laser settings of 2 pre-ablation cleaning shots of $40 \mu\text{m}$ in diameter, 150 ablation shots of $25 \mu\text{m}$ in diameter, for a total analytical time of 73 seconds and pit depth of $\sim 15 \mu\text{m}$. Well-documented zircon standard material 91500 was used as the primary standard, and GJ-1 as a secondary standard to monitor accuracy during the analytical session. Plešovice and Mudtank were used as additional secondary standards (Horstwood, Košler, Gehrels, Jackson, McLean, Paton, & Schoene 2016; Sláma, Košler, Condon, Crowley, Gerdes, Hanchar, Horstwood, Morris, Nasdala, Norberg, Schaltegger, Schoene, Tubrett, & Whitehouse, 2008). Unknowns were normalized to primary standard 91500 (ID-TIMS age of $1062.4 \pm 0.4 \text{ Ma}$, Wiedenbeck, Hanchar, Peck, Sylvester, Valley, Whitehouse, Kronz, Morishita, Nasdala, & Fiebig, 2004), which yielded a concordia age of $1063.1 \pm 5.3 \text{ Ma}$ (MSWD = 0.077). The secondary standard GJ-1 yielded a weighted mean $^{206}\text{Pb}/^{238}\text{U}$ of $600 \pm 4 \text{ Ma}$, MSWD = 0.06, within accepted values for reproducibility within error (ID-TIMS age of $608.5 \pm 0.4 \text{ Ma}$; Jackson, Pearson, Griffin, & Belousova, 2004; LA-ICPMS $^{206}\text{Pb}/^{238}\text{U}$ age of $602 \pm 5 \text{ Ma}$; Horstwood *et al.*, 2016).

3.4 Microstructures and shape fabric analysis: EBSD, XRCT

Omphacite crystallographic preferred orientation in two dome-core and two dome-margin eclogites was determined by electron backscattered diffraction (EBSD) with a JEOL 6500 FEG-SEM and Oxford Instruments/HKL Channel 5 software in the Characterization Facility of the University of

Minnesota. Analytical conditions were 70° tilt, accelerating voltage of 20 kV, and 20 nA beam current. Representative regions of each thin section were mapped with a 10- μm -step size. EBSD phase maps were used to calculate modal amounts of minerals in each eclogite, supplemented by point-counting owing to poor indexing of symplectite.

One eclogite sample from each of the two localities was scanned using X-Ray Computed Tomography (XRCT) in the Department of Earth & Environmental Sciences, University of Minnesota, to evaluate textural features, including rutile shape fabrics. The samples scanned were ~4 x 2 x 1 cm rectangular billets used for the preparation of petrographic thin sections. Scanning conditions were 160 kV, 22 watts, and a 500 ms integration time. We collected 1440 projections averaging 3 frames at each step to reduce noise, and with a spacing of 25 μm between 2D slices.

4. ECLOGITE BULK COMPOSITION

Major and trace-element composition may provide information about protoliths of the eclogite. It is important to note that if the protoliths were gabbroic rocks, as proposed by Demange (1985), the compositions may have been affected by cumulate and other processes, and therefore comparisons of compositions with extrusive mafic rocks should be viewed in this context. The silica and alkali composition of the dome-margin (Cabardès) eclogite (~48 wt% SiO_2 ; ~2.0-2.4 $\text{Na}_2\text{O}+\text{K}_2\text{O}$) and dome-core (Terme de Fourcaric) eclogite (46-48 wt% SiO_2 ; ~1.8-2.3 $\text{Na}_2\text{O}+\text{K}_2\text{O}$) indicate a mafic protolith (Fig. 2a; Table 2). The retrogressed dome-core eclogite at Le Jounié has the highest SiO_2 value (nearly 50 wt%) of the analyzed samples, although its composition is overall similar to those of less retrogressed eclogite. Low values for loss on ignition (LOI) (~0-0.75 wt%; Table 2) are consistent with the mostly-anhydrous mineral assemblages of the less-retrogressed eclogite. More retrogressed eclogite with amphibole-bearing symplectite and/or texturally-late biotite from both dome-core and dome-margin localities have similar to slightly higher SiO_2 , higher alkali totals, and higher LOI (up to 2.1 wt%).

Dome-core and dome-margin eclogite have similar but slightly different trace-element composition. Trace-element indicators (e.g. TiO_2/Yb vs. Nb/Yb) show a deviation from MORB for most analyzed samples, particularly dome-margin eclogite (Fig. 2b). NMORB-normalized trace-element data show that many elements in eclogite from both localities are enriched (in some cases

>10x) relative to NMORB; e.g. U, Nb, Th, Ba, Pb, Zr, Hf, and the LREE (Fig. 2c, Table 2). Some analyzed eclogites have MREE and HREE abundances similar to those in NMORB, but most are slightly depleted in these elements relative to NMORB. The analyzed eclogites lack a strong arc signature (e.g. no pronounced negative Nb anomaly) and are most variable in highly mobile trace elements. All but one of the analyzed eclogites (a dome-core sample) has a positive Pb anomaly relative to NMORB, and there is a distinct difference in Pb abundance between most of the dome-margin eclogites (strong positive Pb anomaly) and most of the dome-core eclogites (smaller positive Pb anomaly) (Fig. 2c). The dome-core retrogressed eclogite has a similar composition in this respect to dome-margin eclogite. Pb abundance does not correlate with that of chalcophile elements (e.g. Cu, Table 2), and REE abundances do not exhibit a Eu anomaly, so the Pb anomaly is unlikely to have been controlled by sulfides or plagioclase.

5. PETROGRAPHY, MINERAL COMPOSITION AND ZONING

Fresh Terme de Fourcaric (dome-core) eclogite is comprised of garnet (45 modal %) + omphacite (35%) + rutile (4%) + amphibole-plagioclase symplectite (16%) + minor quartz (primarily as inclusions in garnet) (Figs. 1b, 3a; Table 1). Zircon and apatite are accessory phases, and ilmenite occurs locally as a partial replacement of rutile (rims, lamellae). Garnet is subhedral, ~3 mm in diameter, and zoned. The composition of quartz inclusion-rich core regions is 43 mol% almandine (alm), 2 mol% spessartine (sps), 32 mol% pyrope (prp), and 23 mol% grossular (grs); core regions have been interpreted to correspond to prograde, amphibolite-facies garnet (Whitney *et al.*, 2015). Rutile-inclusion-bearing rims are more prp-rich (up to 50 mol%) and lower in alm (36 mol%), grs (14 mol%), and sps (0-1 mol%) compared to the cores (Table 3), and have been interpreted as the eclogite-facies part of the garnets (Whitney *et al.*, 2015). Omphacite has a jadeite content of ~35-36 mol%.

Modal amounts of major phases in the dome-margin eclogite are similar to those of the dome-core eclogite: 45% garnet, 35% omphacite, 15% other (mostly symplectite), although the Cabardès eclogite contains more quartz (5%) and less rutile (1%), the latter with texturally late titanite in some samples (Figs. 1b, 3b; Table 1). Minor epidote (in the matrix and as inclusions in garnet, omphacite), zircon, and apatite also occur (Fig. 4). In more retrogressed eclogite, texturally-late biotite occurs as a

matrix phase and in symplectite with plagioclase after garnet. Hornblende occurs in symplectite with plagioclase, as a texturally-late matrix phase (including as thin rims on garnet), and in thin hornblende-rich veins that cross-cut eclogite. Some retrogressed eclogite also contains titanite rims on rutile as well as late chlorite.

One sample of dome-margin eclogite that was studied in detail (MN16-03) resembles the dome-core eclogite in that garnet has quartz inclusion-rich cores and relatively inclusion-free rim regions; however, in contrast to the dome-core eclogite, garnet in the dome-margin eclogite contains rutile and omphacite inclusions throughout (Figs. 4a, b).

Another dome-margin eclogite sample (MN16-05A) that was studied in detail has two distinct textural domains: one fine-grained (~0.1-0.5 mm intergrown garnet and omphacite) and one coarser-grained (~1-2 mm garnets and omphacite) (Figs. 3b, 4c-f, 5a). Large and small garnet contains inclusions of quartz, omphacite, rutile, apatite, and epidote. Cores are more inclusion-rich relative to rims, although omphacite and rutile inclusions occur throughout, in both core and rim regions (Figs. 4c-e).

In the coarser-grained domain, garnet is essentially unzoned, with only a slight change in Fe and Mg at the boundary between inclusion-rich core and inclusion-poor rim region. Lack of zoning is consistent with the presence of omphacite and rutile inclusions throughout. Typical composition is 47-48 mol% alm, 1% sps, 22-24% prp, and 27-28% grs in the core, with a slight decrease in alm (to 46 mol%) and an increase in prp (up to 27%) near the rim (Figs. 5b-c; Table 3). Grossular exhibits slight patchy zoning, with some regions as high as 30 mol%. Quartz-inclusion-bearing large garnet in eclogite MN16-03A is richer in prp and contains less grs than omphacite-bearing large garnet in MN16-05A: ~47 mol% alm in the core (decreasing to 44%), 2 mol% sps (decreasing to 1%), 30 mol% prp (increasing to 33%), and 21 mol% grs (increasing to 23 mol%) (Table 3).

Small garnet in this eclogite has similar composition, inclusion assemblage, and zoning as large garnet in the same sample, but has more complex zoning patterns. Core regions have slight patchy major- and trace-element zoning that appears to be spatially associated with quartz inclusions (Figs. 5d-e; Fig. 6a). Away from quartz inclusions, typical garnet core composition is ~46 mol% alm, 1% sps, 23-24% prp, and 30% grs; within ~20 μm of quartz inclusions, alm increases (to 48%), sps

remains low (1%), prp increases (to 25-26%), and grs decreases (to 25%). Rim regions exhibit similar compositions as cores: ~47 mol% alm, 1% sps, 24% prp, and 28% grs (Figs. 5d-e; Table 3).

Small garnet in MN16-05A is also zoned in some trace elements (Fig. 6a). Cr exhibits complex, patchy zoning; regions with lower Cr correspond to lower-Mg domains (Figs. 5e, 6a). Rutile, ilmenite, and epidote rims are enriched in Cr. Sc is also zoned: lower in most of the garnet core and higher near the rim, with some patchy areas of higher Sc. In the case of Sc, one of the prp-depleted areas corresponds to lower Sc and one to higher Sc. Small garnet is not appreciably zoned in P or Y.

Garnet in dome-core eclogite is also zoned in trace elements, which show a more complex pattern of compositional changes than major elements (Fig. 6b). For example, the quartz-inclusion-rich core region exhibits variations in Cr that resemble sector zoning or domains influenced by the presence of inclusions. The prp-rich rim region displays wispy zones of higher Cr that are aligned with garnet faces. The highest-Cr phase is rutile; variation in Cr content corresponds to extent of replacement of rutile by ilmenite. Higher Cr can also be seen in thin zones along omphacite rims, outlining the grain boundaries (Fig. 6b). P decreases from the quartz-inclusion-rich core to a relatively inclusion-free outer core and then increases to its highest level near the rim. Small apatite inclusions occur in the garnet core, rim, and matrix, but are rare in the lowest-P zone. Sc also exhibits variation in three domains: low in the quartz-inclusion-rich core, higher in an outer core domain surrounding the inclusion-rich core, and lower near the garnet rim. Rutile is enriched in Sc; rutile partially replaced by ilmenite contains lower Sc than unaltered rutile. Y is highest in the garnet core and outer core region, with slight variation corresponding to locations of inclusions, and decreases near the garnet rim. Apatite and rutile both contain Y.

Omphacite in dome-margin eclogite also has two distinct grain sizes: coarse tabular grains (~1 mm) that coexist with larger garnet and finer grains (~0.2 mm) intergrown with smaller garnet (Fig. 3b). All omphacite analyzed (inclusions, matrix) has 26-30% jadeite component. In the MN16-05A eclogite that contains garnet (large and small) with abundant omphacite inclusions (Figs. 4c-e, 5), inclusions are at the lower end of the range for jadeite content (average 27 mol%) and matrix omphacite is closer to the higher end (average 29 mol%) (Table 3). Some matrix grains are slightly zoned: jadeite content increases from core to rim, matching the trend observed in inclusions in garnet: inclusions in garnet core regions are slightly lower in jadeite than inclusions near the rim (Figs. 5b-e).

Matrix rutile is highly elongate and/or occurs as aggregates of small crystals aligned in chains (Figs. 3bs, 5a). The lineation defined by rutile is parallel to that defined by tabular clinopyroxene (omphacite). Rutile contains Zr, Nb, Fe, and Cr (Table 4).

Quartz is heterogeneously distributed in the rock (Fig. 3b). In quartz-rich domains, small garnet contains abundant quartz inclusions and intergrown matrix quartz (Fig. 4d).

Amphibole occurs as texturally-late Mg-hornblende that is typically intergrown with plagioclase in symplectite, which is most common in the coarse-grained part of the eclogite. Epidote occurs in the matrix and as inclusions in garnet and omphacite. It is subhedral and strongly zoned, with a distinct, bright (in BSE images), pistacite-rich rim (Fig. 4f; Table 3).

6. ZIRCON GEOCHRONOLOGY (SHRIMP II)

Zircon from the dome-core (Terme de Fourcaric) eclogite was previously analyzed in grain mounts for age and trace elements using LA-ICPMS at the University of Clermont-Ferrand; ages were obtained separately from trace-elements using the same zircon grains but slightly different spots on the grains (Whitney *et al.*, 2015). Because most of the zircons in the dome-margin eclogite have very thin (<20 μm) rims, we analyzed zircon grain-mounts with the ANU SHRIMP II (10 μm spot size). We also analyzed dome-core eclogite zircon with the SHRIMP II in order to compare results obtained by the same instrument for zircon in eclogite from both localities.

Zircon in the dome-core eclogite ranges in shape from rounded/equant to elongate and in size from ~50 to 200 μm ; some grains have facets but none are euhedral (Fig. 7a). CL images show that some zircons are zoned, whereas others are largely unzoned. Previous LA-ICPMS analysis revealed a dominant concordia age of 315.2 ± 1.6 Ma (2σ) in zircon rims and most cores (Whitney *et al.*, 2015). In that study, four zircon cores (out of 31 analyses of 16 zircon crystals) yielded ages of *c.* 360 Ma, and two yielded ages of *c.* 450-460 Ma (Figs. 7a, b); the latter had higher Th/U ratios (0.12-0.13) than zircon recording younger ages (0.01-0.1) and were discordant. Analyses of zircon grain mounts from this sample using the ANU SHRIMP II yielded a $^{206}\text{Pb}/^{238}\text{U}$ mean age of 310 ± 1.9 Ma for 26 analyses (Fig. 7c; Table 5). With one exception, Th/U ratios are in the range 0.02-0.08 (Table 5). The one exception has a Th/U of 0.16 for a zircon dated at *c.* 306 Ma, but other zircons with the same age have Th/U <0.1 (Table 5). None of the analyzed zircons yielded ages older than *c.* 317 Ma.

Zircon in the dome-margin eclogite is very heterogeneous in size (50-100 μm), shape, and zoning. CL images show complex, patchy zoning of cores, with some grains exhibiting distinctive sector zoning and other grains displaying an intermediate grey inner core surrounded by a darker grey outer core. Both core domains appear to be recrystallized to varying degrees around the margins of the grains, forming thin (<20 μm) CL-bright rims (Fig. 8a), similar to textures described in the literature as indicative of dissolution-reprecipitation (Corfu, Hanchar, Hoskin, & Kinny, 2003). One zircon grain from the dome-margin eclogite with a sufficiently wide rim for analysis was analyzed on SHRIMP II and yielded an age of 314.1 ± 4.6 Ma (1σ) (Table 6, spot #2.1). This age is associated with a low Th/U ratio of 0.005 (Fig. 8a). A small, mostly CL-bright grain with apparent remnant CL-dark cores appears to be mostly recrystallized, and yielded an age of 305.5 ± 4.3 Ma (1σ), with a Th/U ratio of 0.006 (Table 6, spot #16.1, Fig. 8a). Analysis of the three youngest zircons in this dataset yielded an age of 310.7 ± 5.5 Ma (2σ , MSWD = 1.2) (Figs. 8b, c, Table 6), and corresponds to two grains with CL-bright rims (spot #2.1, #13.1) and one nearly recrystallized grain (#16.1). Fifteen spots from zircon cores that are CL-dark or from zircon grains that do not exhibit core-rim zoning have a Th/U ratio between 0.122 and 0.471, and yielded a $^{206}\text{Pb}/^{238}\text{U}$ mean age of 446.1 ± 3.5 Ma (2σ , MSWD = 0.53) (Fig. 8c; Table 6). Mixed analyses were not used for calculations, but the $^{206}\text{Pb}/^{238}\text{U}$ dates obtained from these spots consistently span an age domain between the 310.7 ± 5.5 Ma age obtained from the three slightly discordant youngest spots, and the 446.1 ± 3.5 Ma age obtained for the fifteen, mostly concordant, dark-core analyses. Analytical spots that appear to represent only rim-domains on the pre-ablation images (e.g. spots #4.1, 4.2, Fig. 8a) may have incorporated material from the underlying core domains during ablation, resulting in possible mixed values, and were not used for the metamorphic rim age calculation. On zircon grain #4, two spots on CL-bright rims yielded overall young but inconsistent results: apparent rim spot #4.2 yielded a concordant single-spot date of 338.0 ± 7.6 Ma with very low Th/U=0.008, whereas spot #4.1 yielded a slightly discordant but younger date of 325.7 ± 7.5 Ma, with slightly higher Th/U=0.035. Because of the uncertainty of what these dates may represent, they were not included in the age calculation.

7. ZIRCON GEOCHRONOLOGY AND TRACE-ELEMENT ANALYSIS (LASS-ICPMS)

REE abundances in 30 dated zircon crystals were previously determined by LA-ICPMS for the dome-core eclogite (Whitney *et al.*, 2015). Owing to the thinness of the metamorphic rims on dome-margin eclogite zircon, we obtained LASS-ICPMS depth-profiling data, combining U-Pb age and REE data to investigate the history of zircon crystallization of the dome-margin eclogite (Fig. 9).

Of the nine depth-profiled zircon grains analyzed by LASS-ICPMS, two had very thin, low-U, low-Th rims (<3 μm) that did not permit quantitative analysis. Six grains exhibited near-immediate mixed rim-core analyses, with no rim domain plateau. Unmixing of young, CL-bright rims and older CL-dark core domains was not achievable for these analyses. One grain exhibited a quantifiable low-U, low-Th plateau corresponding to a rim domain (similar to the grain shown in Figs. 9a-b), and this plateau was partially extracted from the time-series (Fig. 9c), along with U-Th-Pb age and REE data (Figs. 9c, d; Tables 7, 8, S1).

For the depth-profiled Cabardès eclogite zircon, partial integration of the rim domain yielded an age of 314 ± 13 Ma with a flat HREE slope, whereas partial integration of the outer and inner core subdomains yielded older ages of 383 ± 24 Ma and 414 ± 10 Ma, respectively, and a steep HREE slope with increasing element mass (Fig. 9c). Different grain subdomains were selected based on $^{206}\text{Pb}/^{238}\text{U}$ age along the profile and REE element abundances. The zircon core displays higher Lu abundance (~ 7 ppm Lu) than the rim (<3 ppm Lu) (Fig. 9b). The errors on the ages for the inner and outer core domains are relatively large due to the small number of points sampled for each partial integration. The low abundance of ^{238}U and thin rim (~ 3 μm) also results in a relatively large error. The grain domains corresponding to CL-bright rims are younger than the CL-dark cores of the grains. The Variscan age of *c.* 314 Ma is consistent with the U-Pb ages obtained on the ANU SHRIMP for the CL-bright rims in the dome-margin eclogite. This age is associated with a flat HREE slope, suggesting crystallization of zircon in the garnet stability field. These results are also consistent with the *c.* 315 Ma age associated with flat HREE slopes pervasively preserved in the dome core eclogite (Whitney *et al.*, 2015).

8. ECLOGITE FABRICS

Omphacite crystals in dome-core and dome-margin eclogite have distinct fabrics as defined by crystallographic orientation relative to the foliation and lineation observed in the samples (Fig. 10).

The samples are not oriented geographically, and the crystallographic preferred orientation (CPO) is determined in relation to the planar (MN14-02, MN13-11A) and planar and linear (MN15-05A, MN16-04) internal fabric retrieved from the samples and thin sections. The CPO of omphacite from two analyzed dome-core eclogites (MN14-02, MN13-11A) is characterized by an E-W elongated maximum of $\langle 001 \rangle$ axes and a broad, single point maximum of (010) (Fig. 10a). In contrast, the CPO of omphacite from two analyzed dome-margin eclogite samples (MN15-05A, MN16-04) shows a tight maximum of $\langle 001 \rangle$ and a N-S girdle of (010) (Fig. 10b).

The two eclogites also differ in their rutile shape fabrics. Dome-margin eclogite contains elongate rutile crystals and aggregates of rutile that define a strong lineation parallel to the long axis of omphacite crystals (Figs. 3bs, 11a, b). In contrast, dome-core eclogite does not contain a strong lineation and is instead primarily characterized by a planar fabric defined in part by a faint compositional layering (Fig. 11c). The samples are not oriented in geographic coordinates relative to other dome rocks; nevertheless, results inform the contrasting boundary conditions of deformation that shaped the rutile fabrics while the rocks were at high pressure.

9. THERMOBAROMETRY

P-T conditions for the dome-core eclogite have been previously determined at $\sim 725^\circ\text{C}$, 1.4 GPa by Grt-Cpx and Zr-in-rutile thermometry and a pseudosection contoured for garnet and omphacite composition (Whitney *et al.*, 2015). Demange (1985) calculated conditions of $\sim 700^\circ\text{C}$, 0.9 ± 0.2 GPa for the dome-margin eclogite using jadeite-in-Cpx barometry and Grt-Cpx Fe-Mg exchange thermometry. Another study described a phase diagram (pseudosection) constructed using the whole-rock composition of the Cabardès (dome-margin) eclogite from Demange (1985) and reported *P-T* conditions of $>650^\circ\text{C}$, >1.4 GPa but did not show the phase diagram or describe how it was calculated (Franke *et al.*, 2011). To determine *P-T* conditions of eclogite facies metamorphism of the dome-margin eclogite and compare results with the dome-core eclogite using the same methods, we constructed pseudosections for the least retrogressed dome-margin eclogite and applied Zr-in-rutile and Ti-in-zircon thermometry. We also calculated Grt-Cpx temperatures and produced similar results ($680\text{--}700^\circ\text{C}$) to previous studies with some calibrations of the thermometer (e.g. Berman, Aranovich,

& Pattison, 1995) and higher temperatures (700-740°C) with others (Krogh Ravna, 2000; Nakamura, 2009).

In the dome-margin eclogite, Zr content in rutile does not vary significantly from core to rim (Table 4). The highest Zr contents are in rutile adjacent to ilmenite, as also observed in the dome-core eclogite (Whitney *et al.*, 2015). Temperatures calculated using the Tomkins, Powell, & Ellis (2007) calibration of the Zr-in-rutile thermometer range from ~650°C (core) to ~680°C (rim not near ilmenite) (Table 9) for P estimates similar to those of the dome-core eclogite (1.4 GPa). Using a slightly lower or higher P estimate (1.2, 1.6 GPa) does not change the calculated T significantly (i.e., ± 4 -5°C), as the thermometer is only slightly P -dependent (Fig. 12).

Ti contents of zircon determined by LA-ICPMS are low in dome-margin and dome-core eclogites: an average of 5 ppm in the dome-core ($n = 36$) and an average of 4 ppm in the dome-margin ($n = 25$). The Ti-in-zircon thermometers of Watson, Wark, & Thomas (2006) and Ferry & Watson (2007) yielded $T \sim 680^\circ$ (dome-core) to 660°C (dome-margin).

We calculated pseudosections using the 2017 version of Perple_X (Connolly, 2005; hp11ver database) for the bulk-rock composition determined by XRF analysis for dome-margin eclogite MN16-05A (Table 2). Bulk compositions of subsets of the eclogite were also calculated using mineral compositions and modes determined from EBSD phase maps for textural subdomains as defined by grain size. The main difference in bulk composition between the two domains is that the coarser domain has slightly higher H_2O content owing to the presence of secondary amphibole. Because domain composition is similar to rock composition, we used the XRF-determined bulk composition.

Phase diagrams were calculated for the chemical system MnNCFMAS(H)T. K was not included because it occurs primarily in minor, retrograde biotite and is present in very small amounts in unaltered eclogite ($\ll 1$ wt% K_2O). Silicate and oxide mineral stoichiometry does not indicate the presence of Fe^{3+} , with the exception of epidote, which is $<1\%$ of the mode, so we calculated the diagram only with Fe^{2+} .

Hydrous minerals in the dome-margin eclogite are retrograde, with the possible exception of minor epidote. There is also no record of the prograde history: garnet contains omphacite and rutile inclusions from core to rim, and garnet does not preserve prograde zoning. To account for uncertainty in the amount of H_2O , we calculated several P - T diagrams: one without H as a component (and

therefore without water as a phase) (Fig. 12a), one with a small amount of H₂O (Fig. 12b), and one with H₂O-saturated conditions (not shown). We used the Gt(WPH) solution models for garnet and the Cpx(HP) model for clinopyroxene; the latter gave similar results to the Omp(GHP) model. Isopleths for garnet components (alm, prp, grs), the jadeite component of clinopyroxene (jd), and modes of garnet and omphacite were determined.

All calculated phase diagrams predict a broad stability field for the assemblage garnet + omphacite + rutile + quartz, with a minimum P of ~1.4 GPa at 680-700°C in the anhydrous system (Fig. 12a). At lower P , plagioclase is stable with a more diopside-rich clinopyroxene. In the anhydrous phase diagram, isopleths for mineral compositions (prp, grs, alm, jd) in the Grt-Omp-Rt-Qz field are steep, widely spaced, and do not intersect each other in the range of P - T conditions calculated (Fig. 12a). Garnet Fe and Mg compositions correspond approximately to the measured composition: e.g. 27-28 mol% prp over the calculated P - T range, compared to 24-27% measured, and ~47-48 mol% alm, the same as the measured composition (Table 2; Fig. 5). The measured grs composition does not plot in the P - T range of the eclogite assemblage, and predicted jadeite compositions are lower by ~5-6 mol% than measured compositions. The slope of Zr-in-rutile isopleths is similar to that of the compositional isopleths, so this diagram predicts only minimum P - T conditions (>650°C, >1.4 GPa) for the Grt-Omp-Qz-Rt stability field (Fig. 12a). Despite the lack of relict prograde hydrous phases or evidence for prograde garnet growth in the dome-margin eclogite, the anhydrous diagram is unlikely to be an accurate representation of phase equilibria in the rock and we therefore show the diagram primarily for comparative purposes.

In the phase diagram calculated with a small amount of water, amphibole and epidote (zoisite) are predicted to coexist with garnet, omphacite, rutile, and quartz. Isopleths for garnet and clinopyroxene composition and mode correspond better to measured composition and intersect at ~650-660°C between 1.6 and 1.7 GPa (Fig. 12b). This temperature of intersection is slightly lower than the T calculated by Zr-in-rutile thermometry for rim compositions of ~350 ppm Zr (Table 9); i.e., ~680°C, but is similar to the T calculated by Ti-in-zircon thermometry (Fig. 12b). Predicted conditions are not substantially different for the H₂O-undersaturated phase diagram, as most hydrous phases had reacted out prior to the peak of metamorphism.

10. DISCUSSION

Dome-core and dome-margin eclogites both contain the peak assemblage garnet + omphacite + rutile + quartz but exhibit differences in peak temperature (and possibly pressure), textures, mineral compositions, zircon characteristics, and deformation fabrics (Table 10). We interpret and discuss eclogite P - T - t - d histories in the context of likely protoliths and prograde history, the conditions and age of high- P metamorphism, and variation in strain history in the deep crust prior to exhumation in the migmatite dome. Taken together, these data illuminate the history of crustal thickening and the exhumation of deep orogenic crust, and document the extent to which the Montagne Noire was deeply sourced.

10.1 Eclogite protolith and prograde history

Age, composition, and field relations are consistent with the interpretation that the protoliths of the Montagne Noire eclogite were closely associated with the protoliths of their gneissic host rocks; i.e. the mafic protoliths were intruded into or otherwise emplaced with more felsic continental rocks. Previous workers have proposed a continental tholeiitic basaltic protolith for the dome-margin eclogite (Gebauer & Grunenfeld, 1982; Demange, 1985). It is likely that the protoliths were gabbroic, consistent with heterogeneity in whole-rock and rutile trace-element composition and the presence of abundant inherited zircon. Mafic protoliths were likely emplaced in a continental orogenic setting, and high- P metamorphism was therefore not related to oceanic subduction.

The presence of compositional and textural zoning in garnet of the dome-core eclogite is consistent with a scenario in which the protolith experienced prograde metamorphism during burial and heating to eclogite facies conditions in the deep crust. In contrast, the dome-margin eclogite lacks evidence for prograde metamorphism. Although this might indicate that the protolith was emplaced in the deep crust and therefore did not experience prograde metamorphism, such an interpretation is inconsistent with the steep REE patterns of zircon cores, indicating protolith crystallization in the presence of plagioclase (but not garnet). Another possible explanation for the lack of prograde history is that the protolith of this eclogite was derived from part of a gabbroic intrusion that did not experience prograde metamorphic reactions owing to kinetic barriers to reaction until it attained eclogite-facies P - T conditions.

The inferred magmatic protolith ages of *c.* 470-450 Ma for both eclogites are similar to the protolith ages of Montagne Noire orthogneiss (Roger *et al.*, 2015) as well as other felsic and mafic rocks in the region (e.g. Lardeaux, 2014). Magmatic protolith age is well recorded in zircon cores of the dome-margin eclogite (Fig. 8c), but there is a very sparse record of inherited zircon in the dome-core eclogite (Whitney *et al.*, 2015; this study). A possible explanation for the difference in preservation of protolith zircon is that dome-core eclogite may have interacted with aqueous fluid that facilitated dissolution of magmatic zircon, whereas dome-margin eclogite experienced significantly less water-rock interaction, although it contains minor epidote and was not entirely anhydrous.

10.2 Conditions and age of eclogite-facies metamorphism

Phase diagram calculations predict $P \sim 1.6\text{-}1.7$ GPa for the dome-margin eclogite (Fig. 12), slightly higher than determined for dome-core eclogite (~ 1.4 GPa, Whitney *et al.*, 2015). Pressure estimates for both eclogites are inexact owing to uncertainties in the calculation of pseudosections, but P - T results indicate that eclogite metamorphism occurred at $P \geq 1.4$ GPa for both eclogite. It is not certain, however, that the dome-margin eclogite attained higher P than the dome-core eclogite, particularly as the peak T determined by several methods consistently indicates a lower T (680°C) for the dome-margin than for the dome-core eclogite (725°C).

The age of HP metamorphism is recorded by *c.* 310 Ma zircon in both dome-core and dome-margin eclogite (Figs. 8-10), an age that corresponds to crystallization of zircon in the presence of garnet (flat HREE) and absence of plagioclase. Widespread (re)crystallization of zircon occurred under HP conditions in the dome-core eclogite, resulting in some neocrystallized zircon that does not have inherited cores. In contrast, HP metamorphism had a more limited effect on zircon growth in the dome-margin eclogite, producing narrow rims on inherited cores. The $\sim 45^\circ\text{C}$ higher peak T recorded by dome-core eclogite compared to dome-margin eclogite is likely insufficient to explain the differences in zircon characteristics. Furthermore, differences in deformation are also unlikely to account for variation in zircon (re)crystallization, as both eclogites experienced HP deformation.

The age of HP metamorphism is similar to the oldest U-Th-Pb zircon and monazite ages in Montagne Noire orthogneiss, migmatite, and dome-carapace micaschists (Roger *et al.*, 2015; Trap *et al.*, 2017), indicating that little time separated eclogite facies metamorphism in the deep crust and

emplacement of the deeply-sourced rocks at shallower levels in the dome. 2D and 3D models for dome emplacement under lithospheric extension or transtension are consistent with exhumation of the dome-margin eclogite before the dome-core eclogite (Rey, Teyssier, Kruckenberg, & Whitney, 2011; Rey, Mondy, Duclaux, Teyssier, Whitney, Bocher, & Prigent, 2017; Korchinski, Rey, Mondy, Teyssier, & Whitney, 2018) (Fig. 13), but transport in an ascending dome is so rapid that any differences in age cannot be resolved within the uncertainty of the geochronometers.

10.3 Conditions of deformation in the deep crust

2D and 3D numerical models predict that migmatite domes exhumed under lithospheric extension will have a central, steep high-strain zone that serves as an exhumation channel connecting deep and shallow crustal levels (Rey *et al.*, 2011, 2017). Deep crust is exhumed via this channel, and then spreads out laterally in the mid-shallow crust. In the Montagne Noire, the dome-core eclogite is in a region that has been identified as a steep, high-strain zone (Rabin, Trap, Carry, Fréville, Cenko-Tok, Lobjoie, Goncalves, & Marquer, 2015), and the dome-margin eclogite is located near the boundary of migmatitic gneiss and the dome's schist carapace (Figs. 1b, c). The presence of eclogite at different structural locations provides an opportunity for testing geodynamic models for dome formation and associated processes, including exhumation of deep crust.

Eclogites in both dome-core and dome-margin sites are deformed, but the two eclogite localities record different high- P fabrics (Figs. 10, 11). Omphacite CPO in dome-core eclogite (Fig. 10a) is consistent with a plane strain to possible flattening fabric (consistent with simple shear to transpression kinematics), whereas the strong linear fabric of dome-margin omphacite (Fig. 10b) and rutile shape (Fig. 11b) indicates constrictional strain, consistent with transtension kinematics (cf. Bascou, Tommasi, & Mainprice, 2002). Comparison with 2D numerical models of thickened crust under extension shows that a zone of compression is predicted in the deep crust directly below a zone of normal faulting in the upper crust as a result of the 'collision' of channels of flowing crust that move laterally from either side of the model, then ascend rapidly in a vertical exhumation zone to shallow crustal levels (e.g. Rey *et al.*, 2011, 2017) (Figs. 13a, b). Although 3D fabrics cannot be directly compared with the results of 2D numerical experiments in any detail, the models predict that

a region of the deep-crust is under compression in an overall regime of extension (Fig. 13b), possibly consistent with omphacite CPO in the dome-core eclogite.

Numerical model results for ascent history of deep crust are consistent with P - T - t histories of natural rocks exhumed in migmatite domes (e.g. Norlander, Whitney, Teyssier, & Vanderhaeghe, 2002; Whitney *et al.*, 2004; Duchêne, Aissa, & Vanderhaeghe, 2006), although it may be unusual for evidence for deep-crust deformation to be preserved. We propose that a region of the deep crust was deformed in a compressional or transpressional zone that developed before and during lithospheric extension (Fig. 13b) and that this fabric is preserved now only in eclogite emplaced in the dome core. Eclogite-facies metamorphism occurred in the deep crust of the Variscan orogen, perhaps in part owing to thickening of the foreland crust in response to flowing crust from the internal parts of the orogen. Crustal thickening may have occurred under transpression (Whitney *et al.*, 2015), so there are multiple possible explanations for the HP fabric preserved in the dome-core eclogite. The different fabrics in dome-core and dome-margin eclogite may indicate that one acquired its fabric in the deep-crust compressional/transpressional zone (dome-core) before or during exhumation, whereas the other (dome-margin) deformed under a regional transtensional strain regime (extensional zone in Fig. 13b). During later exhumation, strain was largely taken up by quartzofeldspathic gneiss and amphibole \pm biotite-bearing retrogressed mafic rocks, allowing relict eclogite lenses to retain HP fabrics.

The contemporaneity of high- P (high- T) and high- T (low- P) metamorphism is evidence for the connection between deep and shallow processes; indeed, the peak T recorded by the eclogites (~ 700 °C) is similar to the T recorded by the felsic units during near-isothermal decompression and relatively shallow crystallization of partial melt (~ 700 °C; Trap *et al.*, 2017). In this scenario of a shared history of mafic inclusions and host gneiss, layers of eclogitized mafic rocks were entrained and incorporated into the flowing crust, and some fragments of eclogite were exhumed along with migmatite in both the core and the periphery of the dome. In this case, the dominantly linear and planar/plane strain fabrics preserved in eclogite from the margin and the core of the dome would have been acquired within zones in the deep crust that deformed in constriction or flattening, respectively, either spatially or sequentially.

11. SUMMARY & IMPLICATIONS

Eclogite is well preserved in two locations in the Montagne Noire gneiss dome, but the prevalence of abundant amphibolite with similar bulk-rock composition as eclogite may indicate that much of the dome at current exposure levels was sourced from the deep orogenic crust. Differences in zircon characteristics – extent of preservation of protolith age, presence/absence of prograde metamorphic zircon domains, and extent of (re)crystallization under eclogite-facies conditions – may be related to differences in extent of fluid-rock interaction. Specifically, dome-margin eclogite has a widespread record of zircon inheritance, no evidence for prograde metamorphism, and a minor record of zircon growth during *HP* metamorphism, whereas dome-core eclogite has a sparse record of protolith zircon, a significant record of prograde metamorphism, and evidence for major recrystallization of zircon during *HP* metamorphism.

The two eclogites were deformed in different structural domains of the deep crust, suggesting that they were in distinct locations relative to the exhumation-driving faults in the upper crust. Dome-core eclogite records transpressional deformation that is consistent with convergence of flowing deep crust, whereas dome-margin eclogite records deformation consistent with an overall regime of transtension interpreted to have exhumed the deep crust in a migmatite dome.

The chemical and physical characteristics of rocks exposed in gneiss domes provide important information about the larger crustal flow systems that produce gneiss domes, including deformation conditions in the deep crust. Gneiss domes and their mafic inclusions are significant indicators of the mechanisms, conditions, timing, and magnitude of mass transport of hot crust from near-Moho depths in thickened crust to near-surface levels. Integration of this new dataset on the *P-T-t-d* history of Montagne Noire eclogite with previous results for the age of host gneiss and migmatite indicates that much of the dome was deeply sourced and exhumed at the same time (Fig. 14), although only a few relict refractory rocks record the high-*P* history.

These results from the Montagne Noire dome may be generally applicable to understanding exhumation of eclogites in migmatite from other orogens, including UHP terrains. Despite some differences in burial and exhumation mechanisms among these terrains, a key shared characteristic is the similarity in age of eclogite and migmatite (e.g. Gordon *et al.*, 2013; Little *et al.*, 2011). If geochronometers in eclogite record *HP* metamorphism rather than a cooling age or later overprint,

these results point to the importance of recognizing dynamic connections between eclogite and migmatite.

Accepted Article

CONFLICT OF INTEREST STATEMENT

The authors confirm that they have no conflicts of interest.

ACKNOWLEDGEMENTS

We acknowledge funding from the National Science Foundation (EAR-1050020) to Teyssier and Whitney, and research support from the College of Science and Engineering at the University of Minnesota. Funding for electron microprobe facility used in this research was provided by NSF grant EAR-1625422. The X-Ray Computed Tomography facility was funded by a UMN Infrastructure Investment Initiative grant. EBSD analyses were carried out in the Characterization Facility of the College of Science and Engineering, University of Minnesota, which receives partial support from NSF through the MRSEC program. We thank Andrew Kylander-Clark for assistance with LA-ICPMS analyses at UC-Santa Barbara, C. Mark Fanning for assistance with SHRIMP analyses at the Australian National University, Ashley Steiner and Charles Knaack for assistance with XRF and ICP-MS analyses at WSU, and Besim Dragovic and Philippe Goncalves for advice about phase diagram calculations. Finally, we thank Mr. Daniel Daures of Le Teil Farm for helping us search for eclogite in the Cabardès area, we thank Mr. Robert Pistre and the Centre de Recherche du Patrimoine de Rieumontagné (CRPR), as well as the association Les Amis des Sciences de la Nature (ASNAT), for having preserved, digitized, and made available a number of Professor M. Demange's unpublished maps and documents that proved critical in our quest for the Montagne Noire eclogites.

REFERENCES

- Aerden, D. G. A. M. (1998). Tectonic evolution of the Montagne Noire and a possible orogenic model for syncollisional exhumation of deep rocks, Variscan belt, France. *Tectonics*, 17, 62–79.
- Alabouvette B., Demange M., Guérangé-Lozes, J., & Ambert, P. (1993). Carte géologique de la France (1/250 000), feuille Montpellier (38). Orléans: BRGM, 165 p.
- Armstrong, J. T. (1988) Quantitative analysis of silicates and oxide minerals: Comparison of Monte-Carlo, ZAF and Phi-Rho-Z procedures. *Microbeam Analysis*, 239-246.
- Baldwin, S. L., Webb, L. E., & Monteleone, B. D. (2008) Late Miocene coesite-eclogite exhumed in the Woodlark Rift. *Geology*, 36, 735–738.
- Bascou, J., Tommasi, A., & Mainprice, D. (2002) Plastic deformation and development of clinopyroxene lattice preferred orientations in eclogite. *Journal of Structural Geology*, 24, 1357-1368.
- Berman, R. G., Aranovich, L. Y., & Pattison, D. R. M. (1995). Reassessment of the garnet-clinopyroxene Fe-Mg exchange thermometer, 2. Thermodynamic analysis. *Contributions to Mineralogy and Petrology*, 119, 30-42.
- Black, L. P., Kamo, S. L., Allen, C. M., Aleinikoff, J. N., Davis, D. W., Korsch, R. J., & Foudoulis, C. (2003). TEMORA 1: a new zircon standard for Phanerozoic U–Pb geochronology. *Chemical Geology*, 200, 155-170.
- Bouchardon, J. L., Déchomets, R., & Demange, M. (1979). A propos du disthène en roche dans les micaschistes et les gneiss du synclinal de Rosis et du flanc sud, zone axiale de la Montagne Noire (Massif Central français). *Comptes Rendus de l'Académie des Sciences, Série D*, 288, 1067-1071.
- Brueckner, H.K. (2018). The great eclogite debate of the Western Gneiss Region, Norwegian Caledonides: The in situ crustal v. exotic mantle origin controversy. *Journal of Metamorphic Geology*, 36, 517-527. DOI: 10.1111/jmg.12314
- Cabanis, B., & Godard, G. (1987). Les écolgites du pays de Léon (Nord-Ouest du Massif Armoricaïn) : étude pétrologique et géochimique; implications géodynamiques. *Bulletin de la Société Géologique de France*, 8 (III, no. 6), 1133-1142.

- Carswell, D. A., Brueckner, H. K., Cuthbert, S. J., Mehta, K., & O'Brien, P. J. (2003). The timing of stabilization and the exhumation rate for ultra-high pressure rocks in the Western Gneiss Region of Norway. *Journal of Metamorphic Geology*, 21, 601-612.
- Cocherie, A., Baudin, T., Autran, A., Guerrot, C., Fanning, C.M., & Laumonier, B. (2005). U-Pb zircon (ID-TIMS and SHRIMP) evidence for the early Ordovician intrusion of metagranites in the late Proterozoic Canaveilles Group of the Pyrenees and the Montagne Noire (France). *Bulletin de la Société Géologique de France*, 176, 269-282.
- Connolly, J. A. D. (2005). Computation of phase equilibria by linear programming: a tool for geodynamic modeling and an application to subduction zone decarbonation. *Earth and Planetary Science Letters*, 236, 524-541.
- Corfu, F., Hanchar, J. M., Hoskin, P. W. O., & Kinny, P. (2003). Atlas of zircon textures. In J. M. Hanchar & P. W. O. Hoskin (Eds.), *Reviews in Mineralogy and Geochemistry*, 53, 469-500.
- Corrie, S. L., Kohn, M. J., & Vervoort, J. D. (2010). Young eclogite from the Greater Himalayan Sequence, Arun Valley, eastern Nepal: P-T-t path and tectonic implications. *Earth and Planetary Science Letters*, 289, 406-416.
- Cottle, J.M., Jessup, M.J., Newell, D.L., Horstwood, M.S.A., Noble, S.R., Parrish, R.R., Waters, D.J., & Searle, M.P. (2009). Geochronology of granulitized eclogite from the Ama Drime Massif: implications for the tectonic evolution of the South Tibetan Himalaya. *Tectonics*, 28, TC1002, doi: 10.1029/2008TC002256.
- Cuthbert, S. J., Carswell, D. A., Krogh Ravn, E. J., & Wain, A. (2000.) Eclogites and eclogites in the Western Gneiss Region, Norwegian Caledonides. *Lithos*, 52, 165-195.
- Demange, M. (1985). The eclogite-facies rocks of the Montagne Noire, France. *Chemical Geology*, 50, 173-188.
- Demange, M. (1999). Evolution tectonique de la Montagne Noire: un modèle en transpression. *Comptes Rendus de l'Académie des Sciences*, 329, 823-829.
- Demange, M., Guérangé-Lozes, J., & Guérangés, B. (1996). Carte géologique de Lacaune et sa notice. *Carte géologique de la France au 1:50 000 n8987*. Bureau de Recherches Géologiques et Minières, Orléans, France.
- Droop, G. T. R. (1987) A general equation for estimating Fe³⁺ concentrations in ferromagnesian

silicates and oxides from microprobe analyses, using stoichiometric criteria. *Mineralogical Magazine*, 51, 431-435.

Ducrot, J., Lancelot, J.R., & Marchand, J. (1983). Datation U-Pb sur zircons de l'éclogite de la Borie (Haut-Allier, France) et conséquences sur l'évolution ante-hercynienne de l'Europe occidentale. *Earth Planetary Science Letters*, 62, 385-394.

Duchêne, S., Aissa, R., & Vanderhaeghe, O. (2006). Pressure-temperature-time evolution of metamorphic rocks from Naxos (Cyclades, Greece): constraints from thermobarometry and Rb/Sr dating. *Geodinamica Acta*, 19, 301–321.

Eskola, P. (1921). On the eclogites of Norway. Videnskapsselskapets Skrifter. I. Matematisk–naturvidenskabelig Klasse, 8, 1–121.

Faure, M., Cocherie, A., Bé Mézème, E., Charles, N., & Rossi, P. (2010). Middle Carboniferous crustal melting in the Variscan belt: new insights from U-Th-Pb monazite and U-Pb zircon ages of the Montagne Noire Axial Zone (southern French Massif Central). *Gondwana Research*, 18, 653-673.

Faure, M., Cocherie, A., Gaché, J., Esnault, C., Guerrot, C., Rossi, P., Wei, L., & Qiuli, L. (2014). Middle Carboniferous intracontinental subduction in the Outer Zone of the Variscan Belt (Montagne Noire Axial Zone, French Massif Central): multimethod geochronological approach of polyphase metamorphism. In K. Schulmann, J. R. Martinez Catalan, J. M. Lardeaux, V. Janousek, and G. Oggiano (Eds.), *The Variscan Orogeny: Extent, Timescale and the Formation of the European Crust. Geological Society of London Special Publication*, 405, doi 10.1144/SP405.2.

Ferry, J. M., & Watson, E. B. (2007). New thermodynamic models and revised calibrations. for the Ti-in-zircon and Zr-in-rutile thermometers. *Contributions to Mineralogy and Petrology*, 154, 429-437.

Franke, W., Doublier, M. P., Klama, K., Potel, S., & Wemmer, K. (2011). Hot metamorphic core complex in a cold foreland. *International Journal of Earth Science*, 100, 753-785.

Fréville, K., Cenki-Tok, B., Trap, P., Rabin, M., Leyreloup, A., Régnier, J.-L., & Whitney, D. L. (2016). Thermal interaction of middle and upper crust during gneiss dome formation: example from the Montagne Noire (French Massif Central). *Journal of Metamorphic Geology*, 34, 447-462. doi:10.1111/jmg.12188

- Gaggero, L., Buzzi, L., Haydoutov, I., & Cortesogno, L. (2009). Eclogite relics in the Variscan orogenic belt of Bulgaria (SE Europe). *International Journal of Earth Sciences*, 98, 1853-1877. doi: 10.1007/s00531-008-0352-x.
- Gebauer, D. & Grunenfelder, M. (1982). Geological development of the Hercynian belt of Europe based on age and origin of high grade and high pressure mafic and ultramafic rocks. *First International Conference on Geochronology, Cosmochronology, Isotope Geology*, Nikko, pp. 111-112.
- Gordon, S.M., Whitney, D.L., Teyssier, C., & Fossen, H. (2013). U-Pb dates and trace-element geochemistry of zircon from migmatite, Western Gneiss Region, Norway: Significance for history of partial melting in continental subduction. *Lithos*, 170-171, 35-53.
- Géze, B. (1949). Etude géologique de la Montagne Noire et les Cévennes méridionales. *Mémoires de la Société Géologique de France, Nouvelle Série*, 29, 215 pp.
- Groppo, C., Lombardo, B., Rolfo, F., & Pertusati, P. (2007) Clockwise exhumation path of granulitized eclogites from the Ama Drime range (eastern Himalayas). *Journal of Metamorphic Geology*, 25, 51-75.
- Hill, E. J., & Baldwin, S. L. (1993) Exhumation of high-pressure metamorphic rocks during crustal extension in the D'Entrecasteaux region, Papua New Guinea. *Journal of Metamorphic Geology* 11, 261–277.
- Horstwood, M. S. A., Košler, J., Gehrels, G., Jackson, S. E., McLean, N. M., Paton, C., & Schoene, B. (2016). Community-derived standards for LA-ICP-MS U-(Th-)Pb geochronology – Uncertainty propagation, age interpretation and data reporting. *Geostandards and Geoanalytical Research*, 40, 311-332.
- Jackson, S. E., Pearson, N. J., Griffin, W. L., & Belousova, E. A. (2004). The application of laser ablation-inductively coupled plasma-mass spectrometry to in situ U/Pb zircon geochronology. *Chemical Geology*, 211, 47-69.
- Johnson, D., Hooper, P., & Conrey, R. (1999). XRF method XRF analysis of rocks and minerals for major and trace elements on a single low dilution Li-tetraborate fused bead. *Advances in X-ray Analysis*, 41, 843-867.
- Korchinski, M., Rey, P. F., Mondy, L., Teyssier, C., & Whitney, D. L. (2018). Numerical

- investigation of deep-crust behavior under lithospheric extension. *Tectonophysics*, 726, 137-146.
- Krogh Ravn, E. (2000). The garnet-clinopyroxene Fe^{2+} - Mg^{2+} geothermometer: an updated calibration. *Journal of Metamorphic Geology*, 18, 211-219.
- Kylander-Clark, A. R. C., Hacker, B. R., & Cottle, J. M. (2013). Laser-ablation split-stream ICP petrochronology. *Chemical Geology*, 345, 99-112.
- Labrousse, L., Prouteau, G., & Ganzhorn, A.-C. (2011). Continental exhumation triggered by partial melting at ultrahigh pressure. *Geology*, 39, 1171-1174.
- Lappin, M. A., & Smith, D. C. (1978). Mantle-equilibrated orthopyroxene eclogite pods from the Basal Gneisses in the Selje District, Western Norway. *Journal of Petrology*, 19, 530–584. <https://doi.org/10.1093/petrology/19.3.530>
- Lardeaux, J. M. (2014). Deciphering orogeny: a metamorphic perspective. Examples from the European Alpine and Variscan belts. Part II. Variscan metamorphism in the French Massif Central – A review. *Bulletin de la Société Géologique de France*, 185, 281-310.
- Little, T. A., Hacker, B. R., Gordon, S. M., Baldwin, S. L., Fitzgerald, P. G., Ellis, S., & Korchinski, M. (2011) Diapiric exhumation of Earth's youngest (UHP) eclogites in the gneiss domes of the D'Entrecasteaux Islands, Papua New Guinea. *Tectonophysics*, 510, 39-68.
- Ludwig, K. R. (2001). Squid 1.02: A user's manual. *Berkeley Geochronology Center Special Publication 2*, 19 p.
- Matte, P., Lancelot J., & Mattauer, M. (1998). La Zone axiale hercynienne de la Montagne Noire n'est pas un "metamorphic core complex" extensif mais un anticlinal post-nappe à coeur anatectique. *Geodinamica Acta*, 11, 13-22.
- Mattinson, C. G., Wooden, J. L., Liou, J. G., Bird, D. K., & Wu, C. L. (2006). Age and duration of eclogite-facies metamorphism, North Qaidam HP/UHP terrane, western China. *American Journal of Science*, 306, 683-711. doi 10.2475/09.2006.01.
- Nakamura, D. (2009). A new formulation of garnet-clinopyroxene geothermometer based on accumulation and statistical analysis of a large experimental dataset. *Journal of Metamorphic Geology*, 27, 495-508.

- Norlander, B. H., Whitney, D. L., Teyssier, C., & Vanderhaeghe, O. (2002) High temperature decompression of the Shuswap metamorphic core complex, Canadian Cordillera. *Lithos*, *61*, 103-125.
- O'Brien, P. J., & Carswell, D. A. (1993) Tectonometamorphic evolution of the Bohemian Massif – evidence from high-pressure metamorphic rocks. *Geologische Rundschau*, *82*, 531-555.
- Okay, A. I. (1993) Petrology of a diamond and coesite-bearing metamorphic terrain – Dabieshan, China. *European Journal of Mineralogy*, *5*, 659-575.
- Pearce, J. A. (2008) Geochemical fingerprinting of oceanic basalts with applications to ophiolite classification and the search for Archean oceanic crust. *Lithos*, *100*, 14-48.
- Pitra, P., Poujol, M., van den Driessche, J., Poilvet, J. C., & Paquette, J.-L. (2012). Early Permian extensional shearing of an Ordovician granite: The Saint-Eutrope “C/S-like” orthogneiss (Montagne Noire, French Massif Central). *Comptes Rendus Geoscience*, *344*, 377-384.
- Rabin M., Trap P., Carry N., Fréville K., Cenko-Tok B., Lobjoie C., Goncalves P., & Marquer D. (2015). Strain partitioning along the anatectic front in the Variscan Montagne Noire massif (Southern French Massif Central). *Tectonics*, *34*, 1709-1735. doi: 10.1002/2014TC003790.
- Rey P. F., Teyssier C., Kruckenberg S. C., & Whitney, D. L. (2011). Viscous collision in channel explains double domes in metamorphic core complexes. *Geology*, *39*, 387-390.
- Rey, P. F., Mondy, L., Duclaux, G., Teyssier, C., Whitney, D. L., Bocher, M., & Prigent, C. (2017). The origin of contractional structures in extensional gneiss domes. *Geology*, *45*, 263-266, doi:10.1130/G38595.1
- Roger, F., Respaut, J. P., Brunel, M., Matte, P., & Paquette, J. L. (2004). Première datation U–Pb des orthogneiss ocellés de la zone axiale de la Montagne Noire (Sud du Massif Central): nouveaux témoins du magmatisme ordovicien dans la chaîne varisque. *Comptes Rendus Geosciences*, *336*, 19–28.
- Roger, F., Teyssier, C., Respaut, J.-P., Rey, P. F., Jolivet, M., Whitney, D. L., Paquette, J.-L., Brunel, M., & Matte, P. (2015). Emplacement of anatectic granite during Variscan extension and exhumation of the Montagne Noire double dome, French Massif Central, France. *Tectonophysics*, *640-641*, 53-69.

- Schuiling, R. D. (1960). Le dôme gneissique de l'Agout (Tarn et Hérault). *Mémoires de la Société Géologique de France*, 39, 1-59.
- Sláma, J., Košler, J., Condon, D. J., Crowley, J. L., Gerdes, A., Hanchar, J. M., Horstwood, M. S. A., Morris, G. A., Nasdala, L., Norberg, N., Schaltegger, U., Schoene, B., Tubrett, M. N., & Whitehouse, M. J. (2008). Plešovice zircon - A new natural reference material for U-Pb and Hf isotopic microanalysis. *Chemical Geology*, 249, 1-35
- Stipska, P., Schulmann, K., & Powell, R. (2008). Contrasting metamorphic histories of lenses of high-pressure rocks and host migmatites with a flat orogenic fabric (Bohemian Massif, Czech Republic): a result of tectonic mixing within horizontal crustal flow? *Journal of Metamorphic Geology*, 26, 623-646. doi: 10.1111/j.1525-1314.2008.00781.x
- Sun, S. S., & McDonough, W. F. (1989). Chemical and isotopic systematics of oceanic basalts; implications for mantle composition and processes. In A. D. Saunders & M. J. Norry (Eds.), *Magmatism in the ocean basins. Geological Society of London*, 42, 313-345.
- Tera, F., & Wasserburg, G. J. (1972). U-Th-Pb systematics in three Apollo 14 basalts and the problem of initial Pb in lunar rocks. *Earth and Planetary Science Letters*, 14, 281-304.
- Teyssier, C., & Whitney, D. L. (2002). Gneiss domes and orogeny. *Geology*, 30, 1139-1142.
- Thompson, P. H., & Bard, J.-P. (1982). Isograds and mineral assemblages in the eastern axial zone, Montagne Noire (France): implications for temperature gradients and P-T history. *Canadian Journal of Earth Sciences*, 19, 129-141.
- Tomkins, H. S., Powell, R., & Ellis, D. J. (2007). The pressure-dependence of the zirconium-in-rutile thermometer. *Journal of Metamorphic Geology*, 25, 703-713.
- Trap, P., Roger, F., Cenki-Tok, B., & Paquette, J.-L. (2017). Timing and duration of partial melting and magmatism in the Montagne Noire gneiss dome (French Massif Central). *International Journal of Earth Sciences*, 106, 453-476.
- Whitney, D. L., & Evans, B. W. (2010). Abbreviations for names of rock-forming minerals. *American Mineralogist*, 95, 185-187.
- Whitney, D. L., Teyssier, C., & Vanderhaeghe, O. (2004). Gneiss domes and crustal flow. In D. L. Whitney, C. Teyssier, & C. S. Siddoway (Eds.), *Gneiss domes in orogeny, Geological Society of America Special Paper*, 380, 15-33.

- Whitney, D. L., Roger, F., Teyssier, C., Rey, P. F., & Respaut, J.-P. (2015). Syn-collapse eclogite metamorphism and exhumation of deep crust in a migmatite dome: the P-T-t record of the youngest Variscan eclogite (Montagne Noire, French Massif Central). *Earth and Planetary Science Letters*, *430*, 224-234. doi: 10.1016/j.epsl.2015.08.026.
- Wiedenbeck, M., Hanchar, J. M., Peck, W. H., Sylvester, P. J., Valley, J. W., Whitehouse, M. J., Kronz, A., Morishita, Y., Nasdala, L., & Fiebig, J. (2004). Further characterisation of the 91500 zircon crystal. *Geostandards and Geoanalytical Research*, *28*, 9-39.
- Watson, E. B., Wark, D. A., & Thomas, J. B. (2006). Crystallization thermometers for zircon and rutile. *Contributions to Mineralogy and Petrology*, *151*, 413-433.
- Williams, I. S. (1998). U-Th-Pb geochronology by ion microprobe. *Reviews in Economic Geology*, *7*, 1-35.
- Yang, J. S., Wooden, J. L., Wu, C. L., Liu, F. L., Xu, Z. Q., Shi, R. D., Katayama, I., Liou, J. G., & Maruyama, S. (2003). SHRIMP U-Pb dating of coesite-bearing zircon from the ultrahigh-pressure metamorphic rocks, Sulu terrane, east China. *Journal of Metamorphic Geology*, *21*, 561-560.
- Zhao, Z-F., Zheng, Y-F., Chen, R-X., Xia, Q-X., & Wu, Y-B. (2007). Element mobility in mafic and felsic ultrahigh-pressure metamorphic rocks during continental collision. *Geochimica et Cosmochimica Acta*, *71*, 5244-5266.

FIGURE CAPTIONS

Fig. 1. (a) Location of the French Massif Central (MC) and neighboring Variscan massifs in western Europe. The Montagne Noire dome is located at the southern margin of the Massif Central (rectangular box); (b) Simplified geologic map of the Montagne Noire dome showing the ‘double dome’ structure composed of two subdomes (southern: Nore-Somail-Caroux; northern: Laouzas-Espinouse) separated by a high-strain zone and mantled by a schist carapace (Schist X) and nappe complexes. The locations of high-pressure rocks (green stars: eclogites with relict garnet + omphacite; blue star: relict garnet only, no omphacite) and an index mineral (K: kyanite in paragneiss/schist) are indicated, as well as two sites (purple stars) mentioned in the literature (Demange, 1985; Alabouvette *et al.*, 1993; Faure *et al.*, 2014) but that do not contain garnet + omphacite either owing to a non-mafic bulk composition or to pervasive greenschist facies retrogression. Abbreviations of localities: Cab: Cabardès; Ctl: Cantausseil; GdH-A: Gorge d’Heric/Airette; LJ: Le Jounié; TdF-Pey: Terme de Fourcaric-Peyrambert. (c) Schematic N-S cross-section of the dome, showing the steep high-strain zone (HSZ) and the shallowly-dipping decollement (dashed lines) (modified from Rey *et al.*, 2011); dome-core and margin eclogite localities are projected onto the section.

Fig. 2. (a-c) Plots of whole-rock major and trace element abundances of Montagne Noire eclogite (Table 2). A key to most symbols is in (c); (a) $\text{Na}_2\text{O}+\text{K}_2\text{O}$ vs. SiO_2 chart showing that the eclogites had basaltic protoliths. Compositions from Demange (1985) are also plotted for the dome-margin (Cabardès) eclogite and a rock interpreted as an eclogite-facies mafic cumulate (Airette); (b) TiO_2/Yb vs. Nb/Yb plot showing that most of the analyzed Montagne Noire eclogites do not have MORB signatures for these element ratios (after Pearce, 2008); dome-margin eclogite (green symbols) deviates more from MORB composition than does dome-core eclogite (blue symbols), with the exception of the retrogressed dome-core Le Jounié eclogite; (c) NMORB-normalized trace element abundances (normalization values from Sun & McDonough, 1989). Eclogite trace-element signatures vary significantly from NMORB compositions in most elements. Dome-core and dome-margin eclogites have similar trends with respect to NMORB, but most of the analyzed dome-margin eclogites have a greater abundance of fluid-mobile elements (LILE) and LREE and a stronger positive Pb anomaly.

Fig. 3. Images of Montagne Noire eclogite thin sections: (a1, b1) Phase maps derived from EBSD analysis, and (a2, b2) BSE images of thin sections. Note that the dome-margin eclogite has two textural domains – one fine-grained and one coarse-grained – both consisting primarily of garnet + omphacite. The difference in rutile (Rt) shape in the two eclogites is highlighted in the BSE images (a2, b2). The phase map and BSE images for each eclogite are from different thin sections of the same sample.

Fig. 4. (a-e) BSE images of garnet in dome-margin (Cabardès) eclogite; (a-b) Examples of the larger garnets containing abundant quartz inclusions (+ rutile + omphacite) in the cores and relatively inclusion-free rims (MN16-03). Rutile (white phase in BSE images) is distributed throughout garnets and the matrix. (c) Large garnet with abundant omphacite inclusions, in an omphacite-rich matrix (MN16-05A). (d-e) Fine-grained garnet and omphacite from the same sample as (c); garnets in quartz-rich regions have abundant quartz inclusions and garnet in omphacite-rich regions has abundant omphacite inclusions. (f) zoned epidote in omphacite in MN16-05A eclogite. Mineral abbreviations after Whitney & Evans (2010).

Fig. 5. (a) Thin section scan of dome-margin eclogite sample MN16-05A showing the locations of the Mg X-ray maps in b-e; garnets in (b) and (c) are examples of the larger isolated porphyroblasts surrounded by omphacite and quartz, and those in (d) and (e) are in the fine-grained domain with small aggregates of garnet + omphacite. Garnet is annotated with pyrope content (red font), and omphacite (inclusions and matrix) with jadeite content (white font). Zoning profiles are shown for two garnets in the fine-grained domain.

Fig. 6. Garnet trace-element zoning in representative garnets from (a) dome-margin eclogite (MN16-05A, fine-grained domain) and (b) dome-core eclogite (MN13-11A). The garnet in (a) is shown in the BSE image in Fig. 4e and the Mg map in Fig. 5e.

Fig. 7. SHRIMP II zircon geochronology data for dome-core eclogite sample MN13-11A (Terme de Fourcaric, Tdf). (a) representative images of zircon grains from the core eclogite, with annotated spots and associated dates (1σ) and Th/U value, (b) Tera-Wasserburg concordia plot for zircons from the dome-core eclogite, and (c) bar plot of increasing $^{206}\text{Pb}/^{238}\text{U}$ ages and associated histogram and probability-density distributions for full zircon U-Pb age dataset except two points showing Pb-loss (light grey). Internal zircon zoning textures indicated on the x-axis.

Fig. 8. SHRIMP II zircon geochronology data for dome-margin eclogite sample MN16-05B (Cabardès, Cab). (a) representative images of zircon grains, with annotated spots and associated dates (1σ) and Th/U value, (b) Tera-Wasserburg concordia plot for zircons from the dome-margin eclogite, and (c) weighted mean plots in order of increasing $^{206}\text{Pb}/^{238}\text{U}$ ages and associated histogram and probability-density distributions for the three youngest spots with bright CL zoning, and a group of zircon cores with dark CL zoning. Internal zircon zoning textures, indicated on the x-axis.

Fig. 9. LASS-ICP-MS depth profiling of zircon from the dome-margin eclogite sample (a) CL image of internal zonation pattern of zircon grain (zrn-01), (b) schematic cross-sectional view through grain mount showing possible path of the laser through the internal grain structure, (c) plot of $^{238}\text{U}/^{206}\text{Pb}$ age (left y-axis) and associated Lu content, in ppm (right y-axis) along depth profile (x-axis). Darker color bands represent actual portion of the data integrated for the calculation of dates and REE abundances shown in (d); lighter color bands represent the extent of the age isotopic and REE plateaus representative of individual subdomains in the depth-profiled grain, shown in (b), (d) chondrite-normalize REE plot for three partially integrated subsets of the depth-profiling data, showing rim data (red), outer core (cyan) and inner core (royal blue) domains, as well as calculated Best Age and 2σ error.

Fig. 10. EBSD data for omphacite from (a) two dome-core and (b) two dome-margin eclogites. Contoured data represent one point per grain. All pole figures are equal area, lower hemisphere projections; half-width = 10° , cluster size = 5° . L = lineation; S = schistosity (foliation). The dome-margin eclogite has a strong lineation but lineation is not apparent in the dome-core eclogite.

Fig. 11. Rutile shape fabric determined by X-Ray Computed Tomography (XRCT); in these images, taken from rectangular billets, all phases other than rutile have been omitted; (a-b) rutile in the dome-margin eclogite is elongate; (c) rutile in the dome-core eclogite does not have a distinct fabric and is dominated by blocky grains.

Fig. 12. Bulk-composition-specific phase diagrams for the Cabardès (dome-margin) eclogite (MN16-05A) assuming (a) anhydrous conditions, and (b) slightly hydrous conditions. Isopleths are shown for mol% pyrope (prp), almandine (alm), grossular (grs), and jadeite (jd) components. Modeling assuming H₂O-saturation is not significantly different regarding the prediction of likely peak conditions.

Fig. 13. Tectonic scenario for the exhumation of the deep crust in a migmatite dome, based on 2D numerical model results of Korchinski *et al.* (2018). (a) Initial thick crust (60 km) with 800°C Moho, showing the distribution of points of origin of the particles tracked in (b) after 10 million years of lithospheric extension. In (b), two approximately horizontal arrays of particles were traced to their starting points at the beginning of extension. Also shown is the region below the solidus (dashed yellow line) at 10 m.y. and crustal zones that are under compression (owing to the convergent flow of partially molten crust toward the center of the model, below a normal fault in the upper crust) and extension. Particles that were at >50 km depth and >700°C at the start of the model are highlighted (bold border); those that were incorporated in the rising dome of partially molten crust during extension and were exhumed to locations corresponding to the dome core and margin are also highlighted ('dome margin' is here defined as the boundary between regions that were above typical solidus conditions for crustal rocks at some point in their history vs. those that were not). Note that the figures show only part of the 360 km wide x 160 km deep numerical models on which they are based. (c) paths of selected particles from 0 (deep-crust origin) to 10 m.y. (<10 km depth). The shaded region is the envelope of trajectories for all tracked particles that originated in the deep-crust and were exhumed to <10 km in 10 m.y. Extension drives widespread exhumation of the deep crust, and most of the exhuming crust traverses the central high-strain zone from deep to shallow levels.

Fig. 14. Summary of P - T - t data for the two fresh Montagne Noire eclogites and their host rocks. The dome-margin eclogite equilibrated at a lower T (~680°C) than the dome-core eclogite (725°C); peak P is more uncertain but was >1.4 GPa for both, and possibly 1.6-1.7 GPa for the dome-margin eclogite. Eclogites and gneiss record the same protolith age (~450 Ma) and high- T (zircon, monazite) age (~310 Ma), indicating that they have shared a history from deep-crustal metamorphism through rapid exhumation to relatively low- P conditions. A schematic prograde path is shown for the dome-core eclogite, but there is no evidence for prograde metamorphism in the dome-margin eclogite samples analyzed in this study. High-pressure history for the gneiss that hosts eclogite is inferred based on field relations. A schematic path for high- T part of the low- P Schist X (schist carapace, Figs. 1b, c) is also shown.

Table 1. Locations and mineral assemblages of Montagne Noire eclogite.

	location	coordinates*	major mineral assemblage
Terme de Fourcaric	dome core	43.5515N, 2.59068E	Grt-Omp-Rt (minor Qz)
Le Jounié	dome core	43.5659N, 2.64269E	Grt-(Omp*)-Rt-Qz *Amp-Pl pseudomorphs after Omp
Cabardès	dome margin	43.40990N, 2.36215E	Grt-Omp-Rt-Qz (Ep inclusions in Omp)

* datum: WGS84

Table 2. Whole-rock major and trace-element composition of Montagne Noire eclogite.

	CAB* MN16 -01	CAB MN16 -02A	CAB MN16 -03A	CAB MN16 -05A	CAB MN16 -05B	TdF MN13 -11C	TdF MN13 -11D	TdF MN13 -11E	TdF MN14 -02B	TdF MN16 -08	LJ MN13 -08
ox wt%											
SiO ₂	47.40	48.66	47.68	48.13	48.11	46.04	47.76	46.87	46.00	48.00	49.94
TiO ₂	2.69	1.21	1.32	2.41	2.66	1.72	1.40	1.39	1.46	1.24	2.82
Al ₂ O ₃	14.33	8.11	13.69	13.62	14.06	16.39	15.50	16.28	16.48	15.78	13.29
FeO	13.21	10.73	10.99	12.35	12.66	10.72	10.43	10.26	10.67	9.22	12.43
MnO	0.23	0.18	0.18	0.25	0.24	0.19	0.18	0.17	0.18	0.16	0.18
MgO	7.96	17.76	10.85	8.00	8.02	10.62	11.70	11.39	11.34	11.59	8.59
CaO	10.35	9.08	10.46	11.64	10.70	10.73	10.69	10.78	10.50	11.16	9.68
Na ₂ O	1.40	0.53	1.75	1.65	1.83	1.65	1.43	2.07	2.10	2.30	1.07
K ₂ O	0.64	0.41	1.16	0.41	0.57	0.29	0.34	0.01	0.01	0.02	0.51
P ₂ O ₅	0.26	0.17	0.34	0.22	0.27	0.24	0.19	0.18	0.18	0.14	0.39
Total	98.48	96.85	98.41	98.66	99.13	98.58	99.62	99.41	98.86	99.62	98.38
LOI**	0.75	2.08	0.75	0.24	0.30	0.22	0.00	0.00	0.22	0.00	1.07
ppm XRF											
Ni	147	666	281	159	157	248	275	181	168	219	214
Cr	266	1310	553	270	263	636	731	754	750	760	366
V	307	205	197	297	319	239	219	210	206	210	250
Cu	314	12	25	138	93	117	111	87	81	76	76
Zn	123	94	88	125	130	85	78	82	79	78	138
Ga	20	14	17	21	22	16	15	15	14	16	23
ICPM S											
Ba	133.15	19.36	198.09	73.80	117.17	42.61	24	22	15.99	16	65
Th	2.00	0.97	3.52	0.95	2.48	1.57	0.41	0.48	0.45	0.37	2.03
Nb	26.20	8.01	39.02	20.62	25.28	9.44	7.73	7.75	8.20	6.74	19.01
Y	30.02	17.84	22.87	24.72	27.20	36.86	27.91	28.66	31.09	25.73	33.74
Hf	4.80	2.14	2.83	4.46	4.78	3.53	3.05	3.26	3.44	3.04	4.06
Ta	1.73	0.48	1.93	1.40	1.66	0.69	0.59	0.58	0.63	0.52	1.32
U	0.57	0.34	1.42	0.38	0.80	0.39	0.30	0.26	0.28	0.28	0.78
Pb	8.94	2.32	10.80	7.17	5.65	1.05	1.77	1.09	1.05	1.35	5.70
Rb	28.02	13.77	45.54	15.54	25.11	13.18	14.1	0.7	0.71	0.70	7.8
Cs	2.03	4.02	3.69	1.81	3.25	4.45	4.08	0.15	0.14	0.14	0.24
Sr	234.59	23.39	250.68	231.80	188.02	114.27	130	108	100.58	123	107
Sc	36.98	28.19	29.10	35.82	36.44	40.39	36.3	34.6	36.13	30.8	28.0
Zr	183.14	79.50	121.52	169.10	183.02	139.45	117	128	136.58	118	160
La	20.16	11.44	24.09	18.89	24.55	12.48	7.06	6.94	6.12	4.62	29.99
Ce	37.57	22.08	49.46	42.11	52.20	27.53	20.22	17.11	16.01	13.29	41.10
Pr	5.70	3.33	5.82	5.77	7.24	3.66	3.17	2.64	2.50	2.22	7.57
Nd	24.24	14.46	22.80	25.30	30.86	15.82	15.20	12.59	12.00	11.42	32.41
Sm	6.26	3.70	4.95	6.09	7.35	4.33	4.43	1.46	3.86	3.77	8.00
Eu	2.07	1.10	1.66	1.90	2.38	1.49	1.46	1.38	1.40	1.35	2.51
Gd	6.93	3.79	5.00	6.13	6.99	5.75	5.08	5.05	5.09	4.60	8.75
Tb	1.16	0.63	0.80	0.97	1.08	1.09	0.90	0.91	0.94	0.81	1.33

Dy	6.71	3.72	4.75	5.55	6.02	7.10	5.48	5.58	6.01	4.94	7.10
Ho	1.24	0.72	0.92	1.02	1.12	1.48	1.12	1.16	1.24	1.03	1.28
Er	2.95	1.85	2.34	2.51	2.72	3.92	2.93	3.09	3.29	2.74	2.97
Tm	0.39	0.25	0.32	0.32	0.36	0.57	0.43	0.44	0.47	0.39	0.38
Yb	2.24	1.51	1.94	1.88	2.14	3.47	2.67	2.66	2.91	2.41	2.10
Lu	0.33	0.22	0.30	0.28	0.32	0.55	0.41	0.40	0.43	0.37	0.30

* CAB = Cabardès; LJ = Le Jounié; TdF = Terme de Foucaric

Table 3. Representative mineral compositions, Cabardès eclogite (MN16-05A).

	Grt- large	Grt- large	Grt- small	Grt- small	Cpx	Cpx	Ep	Ep
	core	rim	nr qz	rim	matrix	incl	core	rim
SiO ₂	38.98	39.02	38.60	38.61	54.53	54.42	38.23	38.55
TiO ₂	0.05	0.06	0.23	0.06	0.14	0.15	0.21	0.21
Al ₂ O ₃	22.13	22.18	21.78	21.92	7.93	7.23	28.40	28.85
Cr ₂ O ₃	0.02	0.03	< d.l.	0.01	< d.l.	0.05	0.02	0.05
FeO*	21.95	21.85	22.51	22.31	5.46	5.34	5.80	6.34
MnO	0.46	0.42	0.60	0.51	0.05	0.02	0.01	<d.l.
MgO	6.43	6.83	6.73	6.07	10.33	10.68	0.24	0.58
CaO	10.17	9.62	9.16	10.49	17.45	17.95	22.64	22.70
Na ₂ O	0.02	0.02	0.06	0.02	4.09	3.88	<d.l.	0.02
K ₂ O	< d.l.	< d.l.	< d.l.	< d.l.	0.01	<d.l.	<d.l.	<d.l.
total	100.20	100.01	99.67	100.00	99.99	99.72	95.55	97.31
<i>cations/ox#</i>	<i>12</i>	<i>12</i>	<i>12</i>	<i>12</i>	<i>6</i>	<i>6</i>	<i>12.5</i>	<i>12.5</i>
Si	2.99	2.99	2.98	2.98	1.97	1.97	3.05	3.03
Ti	-----	-----	0.01	-----	-----	-----	0.01	0.01
Al	2.00	2.00	1.98	1.99	0.34	0.31	2.67	2.67
Cr	-----	-----	-----	-----	-----	-----	-----	-----
Fe ²⁺	1.41	1.40	1.49	1.45	0.17	0.16	0.39	0.42
Mn	0.03	0.03	0.04	0.01	-----	-----	-----	-----
Mg	0.74	0.81	0.78	0.70	0.56	0.58	0.03	0.07
Ca	0.84	0.79	0.76	0.76	0.68	0.70	1.94	1.91
Na	-----	-----	-----	-----	0.29	0.27	-----	-----
<i>mol%</i>								
alm	47	46	48	48				
sps	1	1	1	1				
prp	24	27	26	26				
grs	28	26	25	25				
jd					30	28		

*FeO reported as total iron. Calculation of cpx stoichiometry using the formulation of Droop (1987) indicates that there is little to no Fe in omphacite.

Table 4. Representative rutile compositions in Montagne Noire eclogite.

	Cabardès	Cabardès	Cabardès	Cabardès	Fourcaric
	MN16-03A	MN16-03A	MN16-05A	MN16-05A	MN13-11A
EMPA*	<i>core</i>	<i>rim</i>	<i>core</i>	<i>rim</i>	<i>rim#</i>
<i>ox. wt%</i>					
TiO ₂	98.96	98.73	99.97	99.79	99.92
Cr ₂ O ₃	0.24	0.31	0.16	0.15	n.a.
FeO	0.28	0.39	0.17	0.37	0.05
ZrO ₂	0.05	0.05	0.05	0.03	0.08
Nb ₂ O ₅	0.54	0.57	0.15	0.15	n.a.
total	100.06	100.06	100.50	100.51	100.04
LA-ICPMS**	avg (n=31)		avg (n=41)		
<i>ppm</i>					
U	0.60		6.39		
Th	0.02		< d.l.		
Si	542		493		
V	1083		1060		
Cr	884		642		
Fe	1509		2555		
Y	0.10		< d.l.		
Zr	303		326		
Nb	1137		1150		
Hf	12		11		
Ta	51		61		
W	98		78		

* EMPA, electron microprobe analysis, University of Minnesota;

** LA-ICPMS: UC-Santa Barbara (*different grains analyzed with each method*)

unzoned part of rutile grain, not near from ilmenite

n.a. = not analyzed

Table 5

SHRIMP II U-Pb results for zircon from dome-core eclogite MN13-11.

Spot no.	U (ppm)	Th (ppm)	Th/U	²⁰⁶ Pb (ppm)	²⁰⁴ Pb/ ²⁰⁶ Pb	f ₂₀₆ (%)	²³⁸ U/ ²⁰⁶ Pb	± 1σ	²⁰⁷ Pb/ ²⁰⁶ Pb	± 1σ	²⁰⁶ Pb/ ²³⁸ U	± 1σ	²⁰⁶ Pb/ ²³⁸ U age (Ma)	± 1σ
1.1	201	11	0.053	8.6	-	0.19	20.10	0.25	0.0542	0.0009	0.0497	0.0006	312.5	3.8
1.2	50	2	0.038	2.1	0.000015	0.17	20.59	0.31	0.0538	0.0018	0.0485	0.0007	305.2	4.6
2.1	149	4	0.024	6.3	-	<0.01	20.24	0.26	0.0519	0.0010	0.0494	0.0006	311.1	3.9
2.2	130	6	0.049	5.5	0.000193	<0.01	20.15	0.26	0.0516	0.0011	0.0497	0.0006	312.6	4.0
3.1	146	7	0.051	6.0	-	0.31	20.71	0.26	0.0549	0.0013	0.0481	0.0006	303.0	3.8
3.2	127	5	0.040	5.5	0.000366	0.21	19.83	0.26	0.0544	0.0011	0.0503	0.0007	316.6	4.0
4.1	105	6	0.054	4.5	0.000023	0.03	20.13	0.27	0.0529	0.0013	0.0497	0.0007	312.5	4.1
4.2	156	8	0.053	6.7	0.000122	0.10	19.94	0.25	0.0535	0.0012	0.0501	0.0006	315.1	4.0
5.1	113	4	0.034	4.9	0.000257	0.57	20.10	0.26	0.0572	0.0013	0.0495	0.0006	311.2	3.9
6.1	171	8	0.050	7.3	-	0.01	20.06	0.25	0.0527	0.0010	0.0498	0.0006	313.6	3.9
6.2	133	4	0.031	5.7	-	<0.01	19.95	0.26	0.0511	0.0011	0.0502	0.0007	315.9	4.1
7.1	130	10	0.079	5.5	-	<0.01	20.35	0.26	0.0507	0.0011	0.0493	0.0006	310.0	4.0
7.2	177	15	0.083	7.5	-	0.01	20.32	0.25	0.0526	0.0010	0.0492	0.0006	309.7	3.8
8.1	151	8	0.056	6.5	-	0.04	20.11	0.26	0.0529	0.0011	0.0497	0.0006	312.7	3.9
8.2	214	13	0.062	9.0	0.000076	<0.01	20.47	0.25	0.0525	0.0009	0.0489	0.0006	307.5	3.7
8.3	140	12	0.084	6.0	0.000115	<0.01	20.22	0.27	0.0518	0.0013	0.0495	0.0007	311.5	4.1
9.1	179	11	0.062	7.4	0.000322	0.05	20.74	0.26	0.0528	0.0011	0.0482	0.0006	303.4	3.8
9.2	104	7	0.065	4.2	-	0.27	21.18	0.29	0.0544	0.0015	0.0471	0.0007	296.6	4.0
10.1	129	6	0.046	5.4	0.000192	0.24	20.40	0.27	0.0545	0.0012	0.0489	0.0007	307.8	4.1
11.1	186	10	0.053	7.8	-	0.04	20.47	0.26	0.0528	0.0010	0.0488	0.0006	307.4	3.8
11.2	72	3	0.045	3.1	0.000615	0.12	20.24	0.29	0.0536	0.0015	0.0493	0.0007	310.5	4.4
12.1	125	4	0.033	5.3	0.000288	<0.01	20.32	0.28	0.0510	0.0014	0.0493	0.0007	310.3	4.2
12.2	210	16	0.078	8.4	0.000372	0.36	21.59	0.28	0.0550	0.0016	0.0462	0.0006	290.9	3.7
13.1	171	12	0.069	7.1	0.000140	0.14	20.63	0.31	0.0536	0.0011	0.0484	0.0007	304.7	4.5
14.1	203	33	0.161	8.5	0.000121	0.31	20.54	0.25	0.0549	0.0009	0.0485	0.0006	305.6	3.7
14.2	120	4	0.031	5.0	-	0.20	20.58	0.27	0.0541	0.0013	0.0485	0.0007	305.2	4.0
15.1	146	6	0.039	6.2	-	0.18	20.18	0.26	0.0540	0.0011	0.0495	0.0006	311.3	4.0
15.2	150	10	0.068	6.4	0.000119	0.11	20.14	0.26	0.0535	0.0011	0.0496	0.0006	312.0	4.0

Notes:

1. Uncertainties given at the 1σ level.
2. Error in Temora reference zircon calibration was 0.37% for the analytical session.
(not included in above errors but required when comparing data from different mounts).
3. f₂₀₆ % denotes the percentage of ²⁰⁶Pb that is common Pb.
4. Correction for common Pb for the U/Pb data has been made using the measured ²³⁸U/²⁰⁶Pb and ²⁰⁷Pb/²⁰⁶Pb ratios following Tera and Wasserburg (1972) as outlined in Williams (1998).
5. Spots 9.2 and 12.2 (grey) are low in radiogenic Pb and were excluded from the dataset for calculations
6. % error on age including internal and external error of 0.37% in Temora reference zircon calibration for the analytical session
where % error = √(((100*Age)/(internal error))² + (0.37)²)

wtd ave dominant **Age** ± internal % error ⁶ ± include std: ie external
310.0 1.5 0.61 **1.9**

MSWD = 0.90 for 26 of 28 areas analysed

Table 6

SHRIMP II U-Pb results for zircon from dome-margin eclogite MN16-05B.

Spot no.	U (ppm)	Th (ppm)	Th/U	²⁰⁶ Pb (ppm)	²⁰⁴ Pb/ ²⁰⁶ Pb	f ₂₀₆ (%)	²³⁸ U/ ²⁰⁶ Pb	± 1σ	²⁰⁷ Pb/ ²⁰⁶ Pb	± 1σ	²⁰⁶ Pb/ ²³⁸ U	± 1σ	²⁰⁶ Pb/ ²³⁸ U age (Ma)	± 1σ
1.1	35	11	0.308	2.2	0.000404	0.43	13.812	0.249	0.0594	0.0024	0.0721	0.0013	448.7	8.0
2.1	47	0	0.005	2.0	-	0.22	19.983	0.297	0.0544	0.0017	0.0499	0.0008	314.1	4.6
2.2	1092	515	0.471	67.6	0.000013	0.05	13.880	0.157	0.0563	0.0003	0.0720	0.0008	448.3	5.0
2.3	400	74	0.184	23.5	0.000023	0.07	14.617	0.167	0.0559	0.0005	0.0684	0.0008	426.3	4.8
3.1	59	15	0.251	3.0	-	0.42	16.722	0.273	0.0575	0.0021	0.0595	0.0010	372.9	6.1
3.2	616	177	0.287	38.0	-	<0.01	13.922	0.235	0.0558	0.0005	0.0718	0.0012	447.2	7.4
4.1	15	1	0.035	0.7	0.003378	3.20	18.681	0.424	0.0787	0.0044	0.0518	0.0012	325.7	7.5
4.2	14	0	0.008	0.7	-	0.44	18.492	0.413	0.0568	0.0035	0.0538	0.0012	338.0	7.6
4.3	510	204	0.400	31.8	-	<0.01	13.804	0.161	0.0554	0.0005	0.0725	0.0009	451.1	5.2
5.1	271	81	0.298	16.5	0.000047	0.06	14.127	0.180	0.0562	0.0009	0.0707	0.0009	440.6	5.5
5.2	121	12	0.097	5.4	0.000428	0.45	19.458	0.262	0.0565	0.0012	0.0512	0.0007	321.6	4.3
5.3	89	15	0.173	5.1	0.002668	6.33	15.079	0.218	0.1056	0.0147	0.0621	0.0015	388.5	9.2
6.1	85	2	0.025	3.8	0.001434	0.77	19.146	0.298	0.0592	0.0017	0.0518	0.0008	325.7	5.0
6.2	46	1	0.012	2.2	-	<0.01	18.228	0.271	0.0521	0.0018	0.0549	0.0008	344.8	5.1
6.3	533	150	0.281	33.0	-	<0.01	13.899	0.167	0.0552	0.0006	0.0720	0.0009	448.2	5.3
7.1	124	16	0.130	5.7	0.000377	0.46	18.810	0.253	0.0568	0.0012	0.0529	0.0007	332.4	4.4
7.2	239	24	0.102	12.3	0.000056	0.41	16.606	0.215	0.0574	0.0010	0.0600	0.0008	375.4	4.8
7.3	458	151	0.331	28.5	0.000047	0.06	13.811	0.168	0.0564	0.0006	0.0724	0.0009	450.4	5.4
8.1	182	36	0.201	10.8	0.000004	<0.01	14.192	0.171	0.0556	0.0009	0.0705	0.0009	439.0	5.2
9.1	52	16	0.308	3.2	0.000711	<0.01	13.898	0.217	0.0537	0.0017	0.0721	0.0011	449.1	6.9
10.1	309	38	0.122	18.7	0.000122	0.08	14.154	0.158	0.0563	0.0007	0.0706	0.0008	439.7	4.8
10.2	71	11	0.160	4.1	0.000046	<0.01	14.758	0.217	0.0528	0.0016	0.0680	0.0010	423.9	6.2
11.1	27	10	0.380	1.6	-	0.23	13.958	0.268	0.0577	0.0024	0.0715	0.0014	445.1	8.5
11.2	50	15	0.305	3.1	0.000803	<0.01	13.858	0.223	0.0538	0.0024	0.0724	0.0012	450.3	7.2
12.1	78	12	0.152	3.7	0.000267	0.29	17.914	0.242	0.0558	0.0013	0.0557	0.0008	349.2	4.7
12.2	312	50	0.161	18.1	0.000127	0.09	14.792	0.174	0.0560	0.0007	0.0675	0.0008	421.3	4.9
12.3	515	164	0.319	31.7	0.000082	0.16	13.957	0.167	0.0571	0.0006	0.0715	0.0009	445.4	5.2
13.2	342	150	0.439	21.1	0.000082	<0.01	13.904	0.171	0.0556	0.0007	0.0719	0.0009	447.9	5.4
13.1	106	17	0.156	4.6	-	0.59	19.939	0.306	0.0574	0.0021	0.0499	0.0008	313.7	4.8
14.1	57	116	2.020	5.9	0.000107	0.39	8.279	0.130	0.0669	0.0015	0.1203	0.0019	732.4	11.2
15.1	66	3	0.038	3.2	0.001205	0.14	17.686	0.258	0.0547	0.0015	0.0565	0.0008	354.1	5.1
15.2	147	54	0.370	9.0	0.000107	<0.01	13.964	0.172	0.0552	0.0009	0.0717	0.0009	446.2	5.4
16.1	71	0	0.006	3.0	0.000887	0.23	20.558	0.289	0.0543	0.0015	0.0485	0.0007	305.5	4.3

Notes:

1. Uncertainties given at the 1σ level.
2. Error in Temora reference zircon calibration was 0.49% and 0.37% for the analytical sessions.
(not included in above errors but required when comparing data from different mounts).
3. f₂₀₆ % denotes the percentage of ²⁰⁶Pb that is common Pb.
4. Correction for common Pb for the U/Pb data has been made using the measured ²³⁸U/²⁰⁶Pb and ²⁰⁷Pb/²⁰⁶Pb ratios following Tera and Wasserburg (1972) as outlined in Williams (1998).
5. % error on age including internal and external error of 0.49% and 0.37% in Temora reference zircon calibration for the analytical sessions where % error = √(((100*Age)/(internal error))² + (0.49)² + (0.37)²)

	Age	± internal	% error ⁵	± include std: ie external	
<u>wld ave dominant grouping</u>	446.1	2.1	0.77	3.5	MSWD = 0.53 for 15 of 33 areas analysed
<u>wld ave youngest 3 analyses</u>	310.7	5.2	1.78	5.5	MSWD = 1.2 for 3 of 33 areas analysed

Table 7

Zircon single grain Th-U-Pb LASS-ICP-MS isotopic data from dome-margin eclogite MN16-05B
 Partial integrations of spectral sub-domains from total depth-profiling data

Composition			Isotopic Ratios													Dates (Ma)				Calculated Ages (Ma)						
Sample	grain domain	# of spots ¹	U (ppm)	Th (ppm)	Th/U	²⁰⁷ Pb / ²³⁵ U	± 2σ	²⁰⁶ Pb / ²³⁸ U	± 2σ	rho	²³⁸ U / ²⁰⁶ Pb	± 2σ	²⁰⁷ Pb / ²⁰⁶ Pb	± 2σ	rho	²⁰⁸ Pb / ²³² Th	± 2σ	²⁰⁶ Pb/ ²³⁸ U	± 2σ	²⁰⁷ Pb/ ²³⁵ U	± 2σ	²⁰⁷ Pb/ ²⁰⁶ Pb	± 2σ	Best age ²	± 2σ	Conc.
MN16-05B	rim	26	56	0	0.000	0.458	0.042	0.051	0.002	0.64	19.685	0.801	0.067	0.006	0.219	-0.008	#####	319	11	381	28	780	170	314	13	0.83
MN16-05B	outer core	6	242	5	0.021	0.489	0.050	0.062	0.004	0.93	16.260	1.031	0.058	0.003	0.291	0.049	0.026	385	23	404	34	520	120	383	24	0.95
MN16-05B	inner core	8	177	1	0.007	0.549	0.041	0.067	0.002	-0.02	14.997	0.366	0.059	0.004	0.339	0.002	0.044	416.1	5.6	444	26	550	140	414	10	0.94

¹ number of spots corresponds to the number of laser pulses corresponding to a specific grain domain used for partial integration of the full depth-profiled time series data

² Best age calculation corresponds to the ²⁰⁷Pb/²⁰⁶Pb corrected ²⁰⁶Pb/²³⁸U age (projected to Concordia). 2σ error includes error propagation

Table 8
Zircon Th-U-Pb LASS-ICP-MS REE data from dome-margin eclogite MN16-05B
Partial integrations of spectral sub-domains from total depth-profiling data

Sample name	Grain domain	# of spots ¹	Calculated Ages (Ma)		REE composition data																														
			Best age ²	± 2σ	Conc.	La (ppm)	± 2σ	Ce (ppm)	± 2σ	Pr (ppm)	± 2σ	Nd (ppm)	± 2σ	Sm (ppm)	± 2σ	Eu (ppm)	± 2σ	Gd (ppm)	± 2σ	Tb (ppm)	± 2σ	Dy (ppm)	± 2σ	Ho (ppm)	± 2σ	Er (ppm)	± 2σ	Tm (ppm)	± 2σ	Yb (ppm)	± 2σ	Lu (ppm)	± 2σ	Hf (ppm)	± 2σ
MN16-05B	rim	26	314	13	0.83	5.8	2.7	2.43	0.96	1.27	0.79	4.4	2.2	1.08	0.70	0.60	0.27	4.4	1.5	1.05	0.34	9.0	2.3	1.57	0.42	4.3	1.1	0.58	0.25	5.0	1.5	0.52	0.22	14900	1100
MN16-05B	outer core	6	383	24	0.95	3.6	4.1	4.60	2.30	0.92	0.34	3.2	3.4	1.10	1.80	0.50	0.77	3.7	4.5	0.88	0.93	7.4	2.6	1.78	0.68	5.9	2.4	1.11	0.60	15.8	6.6	4.10	1.20	12200	2100
MN16-05B	inner core	8	414	10	0.94	bdl	1.0	1.80	1.00	bdl	1.00	bdl	1.0	0.94	0.68	0.25	0.33	2.3	1.5	1.30	0.77	7.0	4.9	3.00	1.60	13.6	4.8	2.90	1.30	43.0	6.4	7.30	3.00	16100	1800

Alternatively (without 2σ errors)

Sample name	Grain domain	# of spots ¹	Calculated Ages (Ma)		REE composition data																
			Best age ²	± 2σ	Conc.	La (ppm)	Ce (ppm)	Pr (ppm)	Nd (ppm)	Sm (ppm)	Eu (ppm)	Gd (ppm)	Tb (ppm)	Dy (ppm)	Ho (ppm)	Er (ppm)	Tm (ppm)	Yb (ppm)	Lu (ppm)	Hf (ppm)	
MN16-05B	rim	26	314	13	0.83	5.8	2.43	1.27	4.4	1.08	0.60	4.4	1.05	9.0	1.57	4.3	0.58	5.0	0.52	14900	
MN16-05B	outer core	6	383	24	0.95	3.6	4.60	0.92	3.2	1.10	0.50	3.7	0.88	7.4	1.78	5.9	1.11	15.8	4.10	12200	
MN16-05B	inner core	8	414	10	0.94	bdl	1.80	bdl	bdl	0.94	0.25	2.3	1.30	7.0	3.00	13.6	2.90	43.0	7.30	16100	

¹ number of spots corresponds to the number of laser pulses corresponding to a specific grain domain used for partial integration of the full depth-profiled time series data

² Best age calculation corresponds to the ²⁰⁷Pb/²⁰⁶Pb corrected ²⁰⁶Pb/²³⁸U age (projected to Concordia). 2σ error includes error propagation

Table 9. Zr content in rutile and calculated temperature.

location	sample#	Zr (ppm)	location of analysis	T °C*
Cabardès	MN16-03A	254	core	654
		358	rim	682
		336	core	676
		364	rim	683
		337	core	677
		(avg LA-ICPMS)	303	
Cabardès	MN16-05A	300	core	667
		423	rim next to Ilm	696
		340	rim	677
		318	core	672
		350	rim	680
		(avg LA-ICPMS)	326	
Terme de Fourcaric **	MN13-11A	521	inclusion in Grt	714
		620	matrix	730
		663	matrix	737

* temperatures shown for pressure estimates of 1.4 GPa and calculation with Tomkins *et al.* (2007) calibration.

** data from Whitney *et al.* (2015)

Table 10. Summary of P-T-t-d characteristics of Montagne Noire eclogites.

	Terme de Fourcaric <i>dome core</i>	Cabardès <i>dome margin</i>
pressure	~1.4 GPa	~1.4 GPa
temperature	~725°C	~680°C
age of HP metamorphism	314.4 ± 2.0 Ma* 315.2 ± 1.6 Ma**	314.1 ± 4.6 Ma
HP zircon Th/U, HREE trend	< 0.1, flat	< 0.1, flat
rutile composition	high Cr, low Nb	low Cr, high Nb
HP deformation regime	transpression	transtension
record of protolith age	~450 Ma (sparse)	~470-450 Ma (widespread)
record of prograde metamorphism	garnet, some zircon (~360 Ma**)	not observed
≥ 360 Ma zircon Th/U, HREE	>0.2, steep	variable, steep

* this study ; ** Whitney et al. (2015)

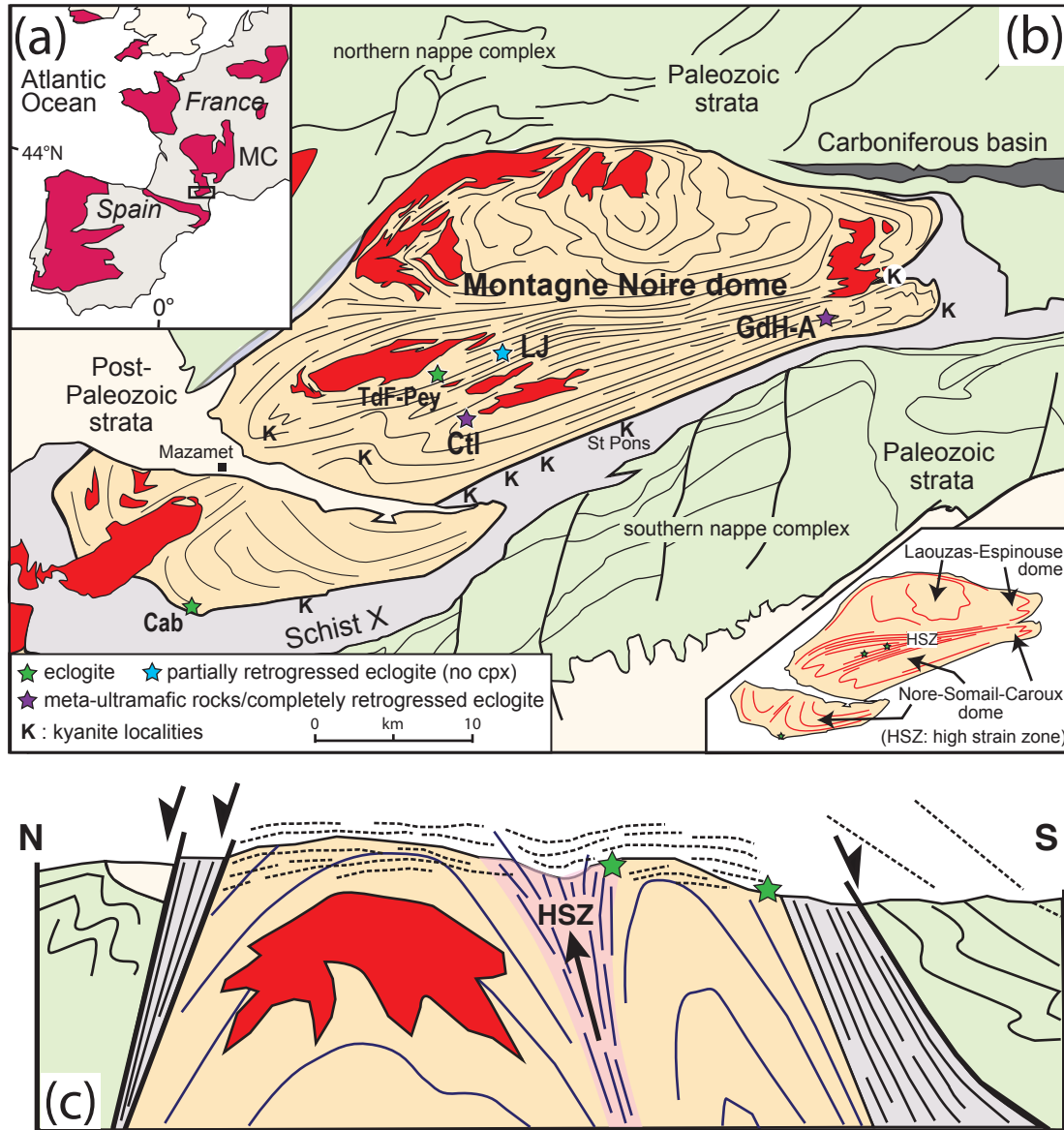


Figure 1

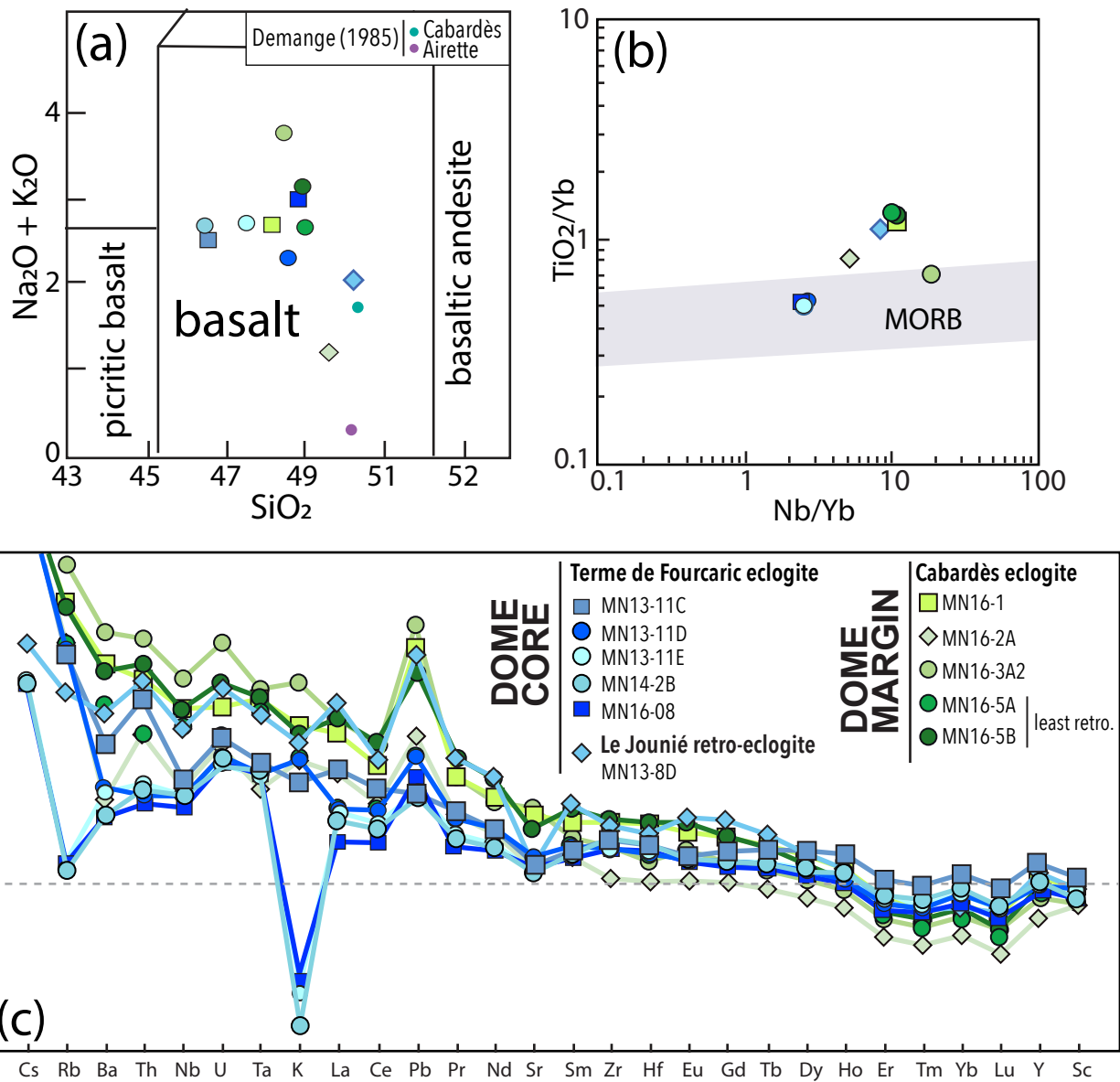


Figure 2

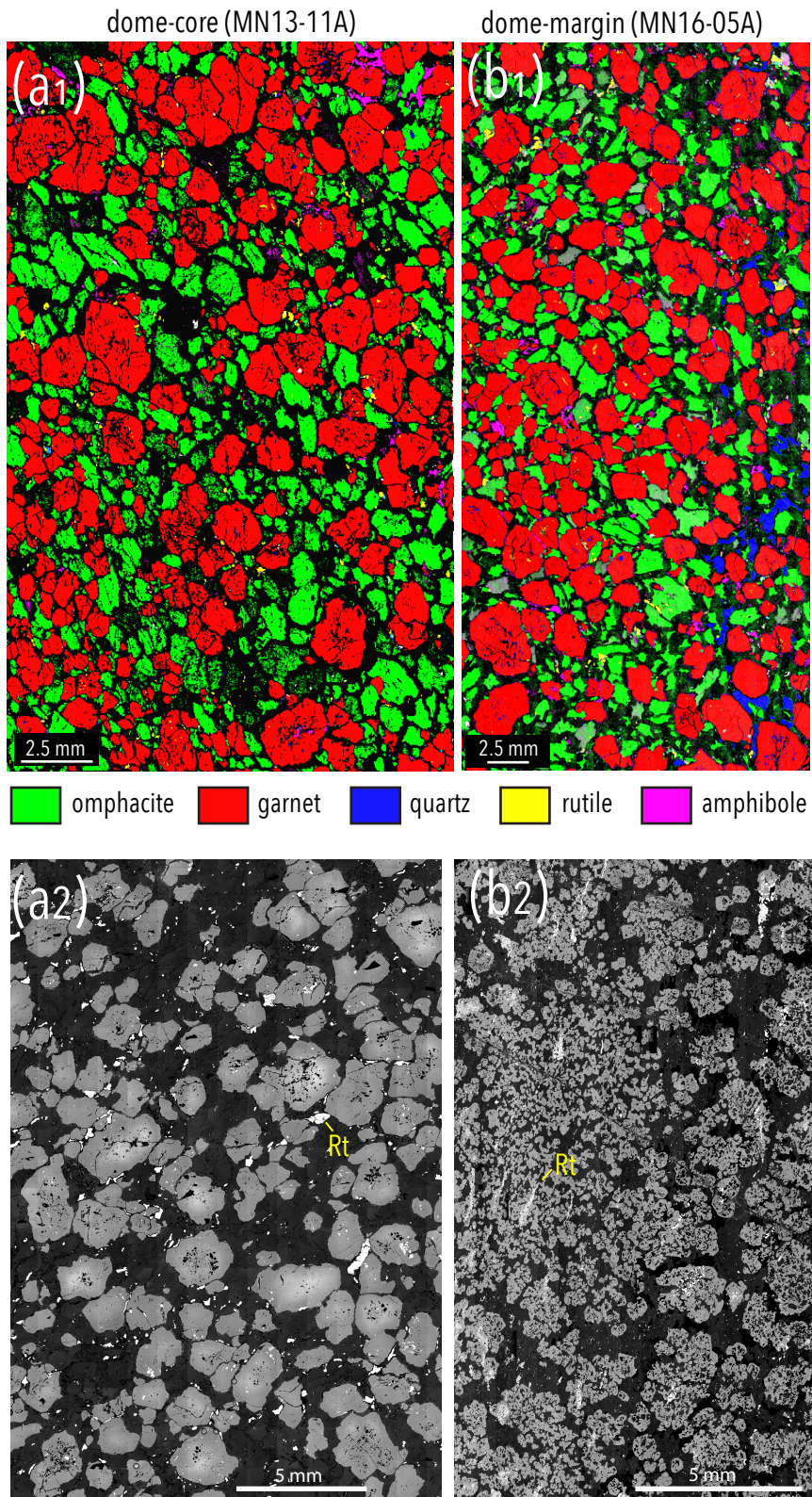


Figure 3

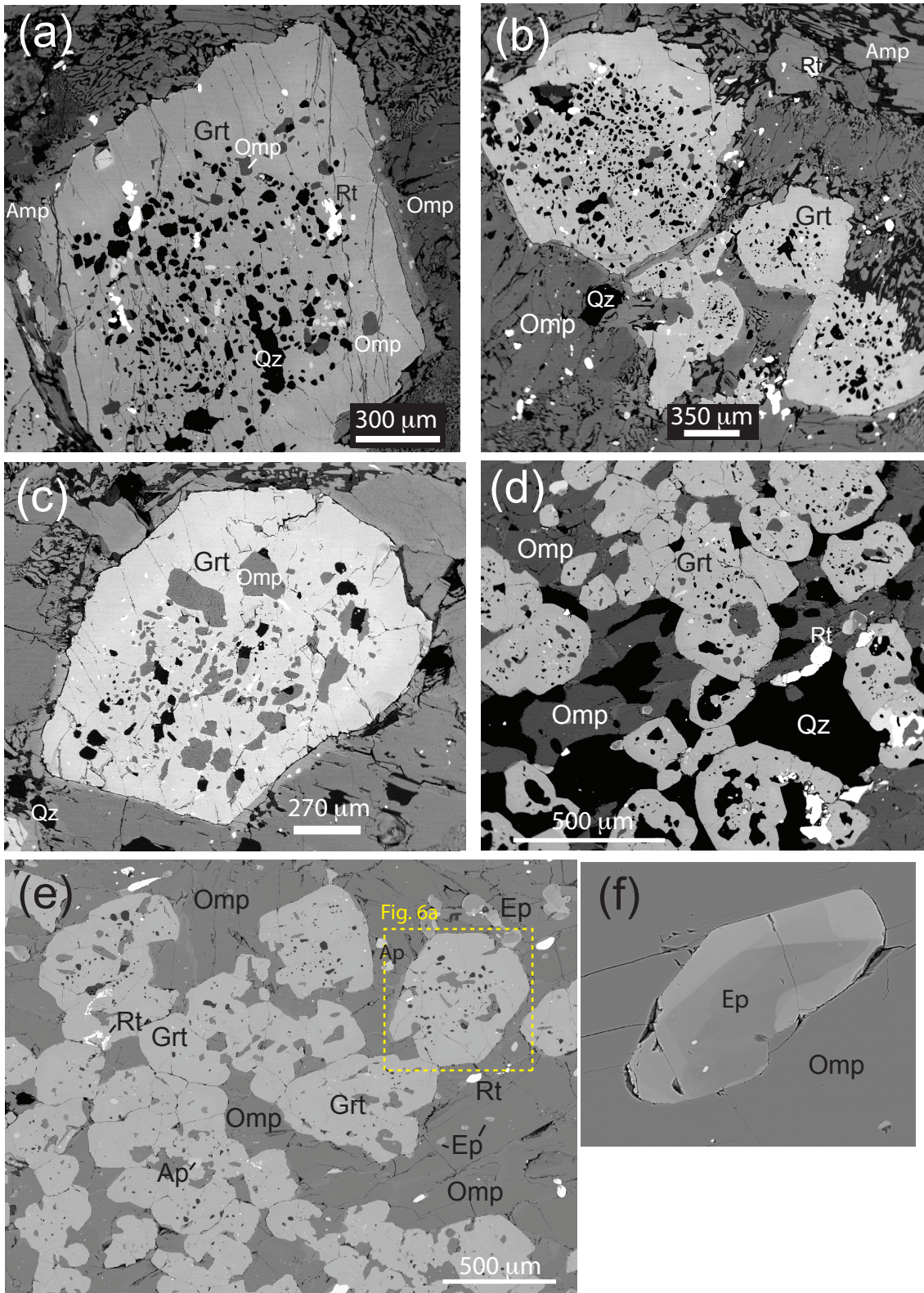


Figure 4

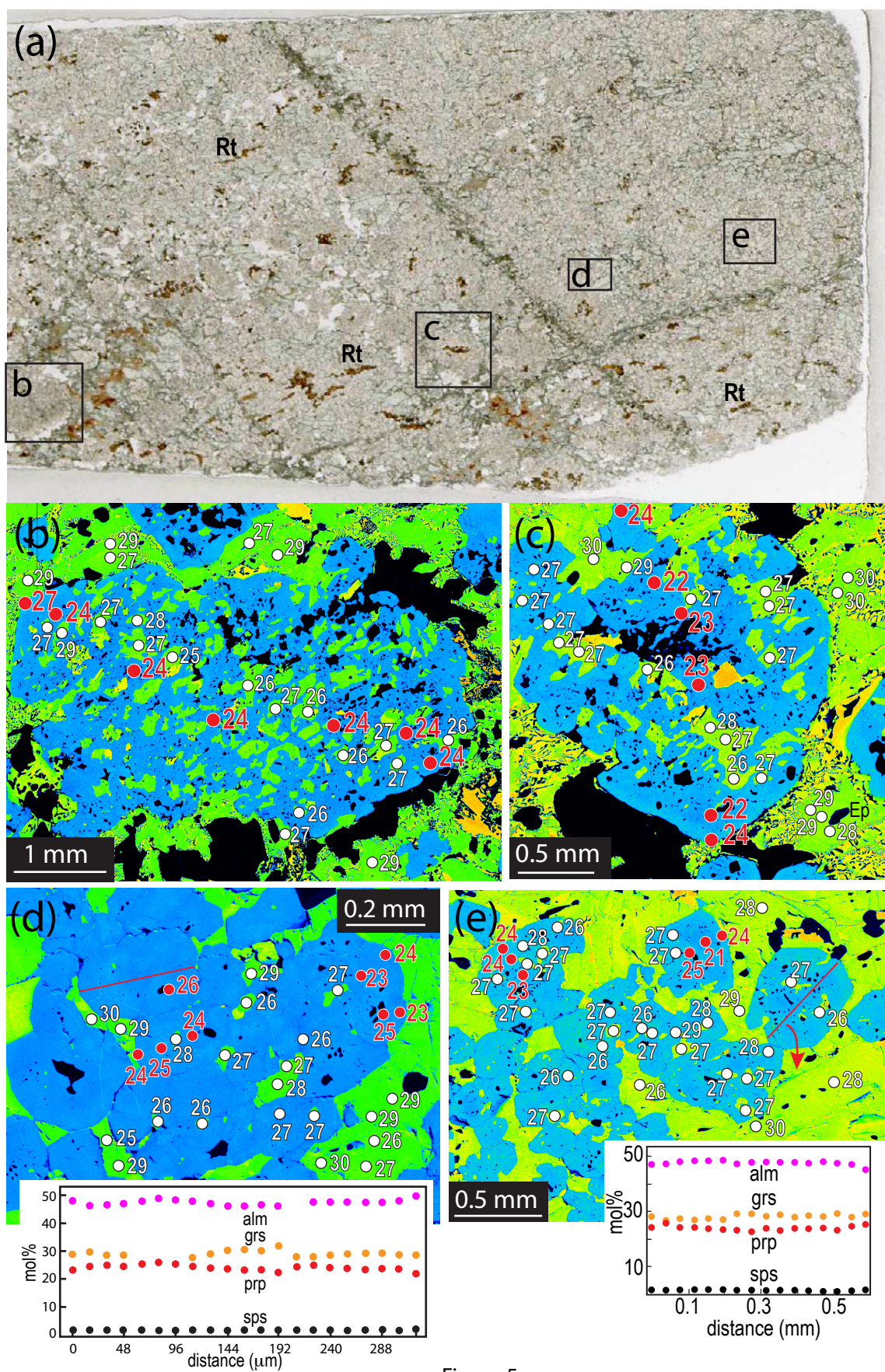


Figure 5

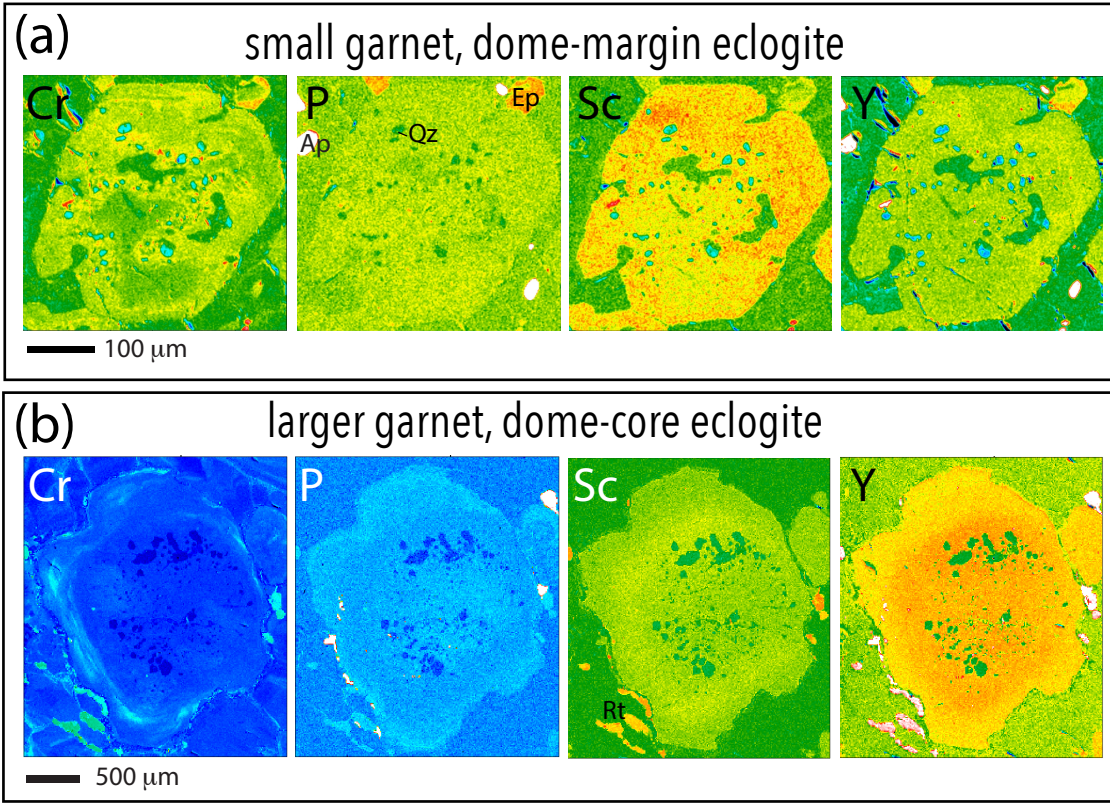
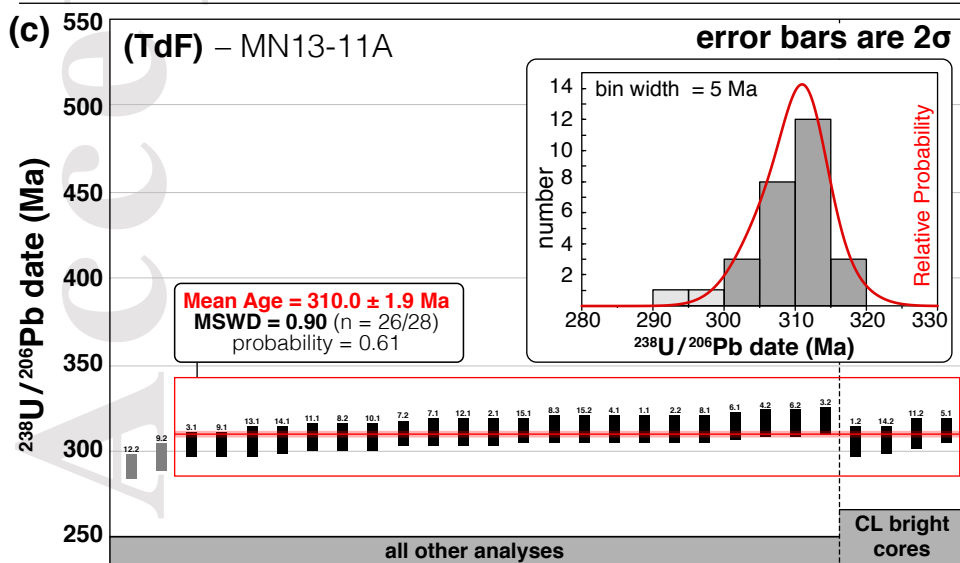
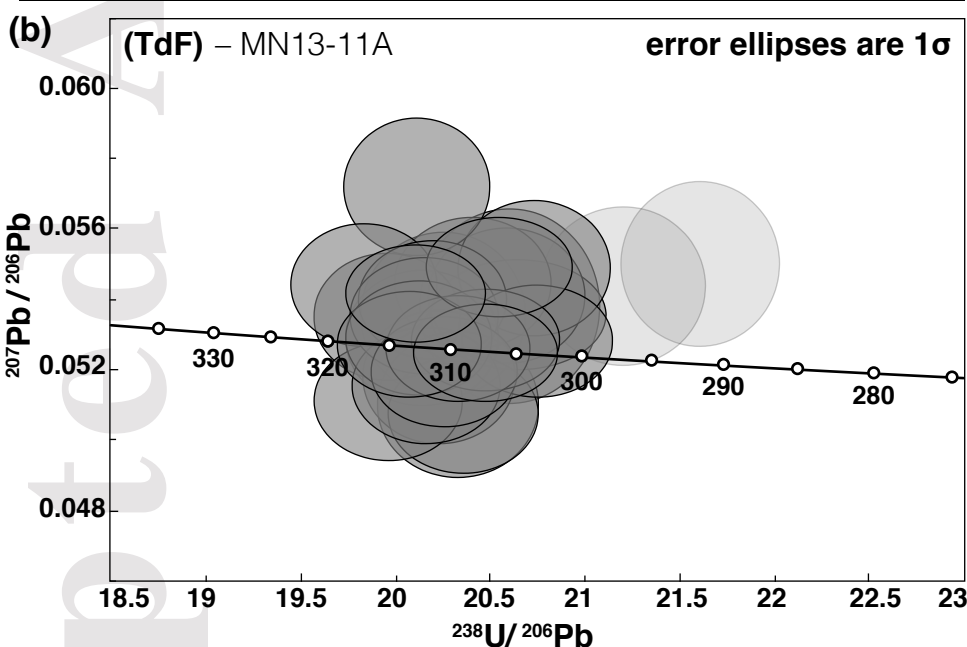
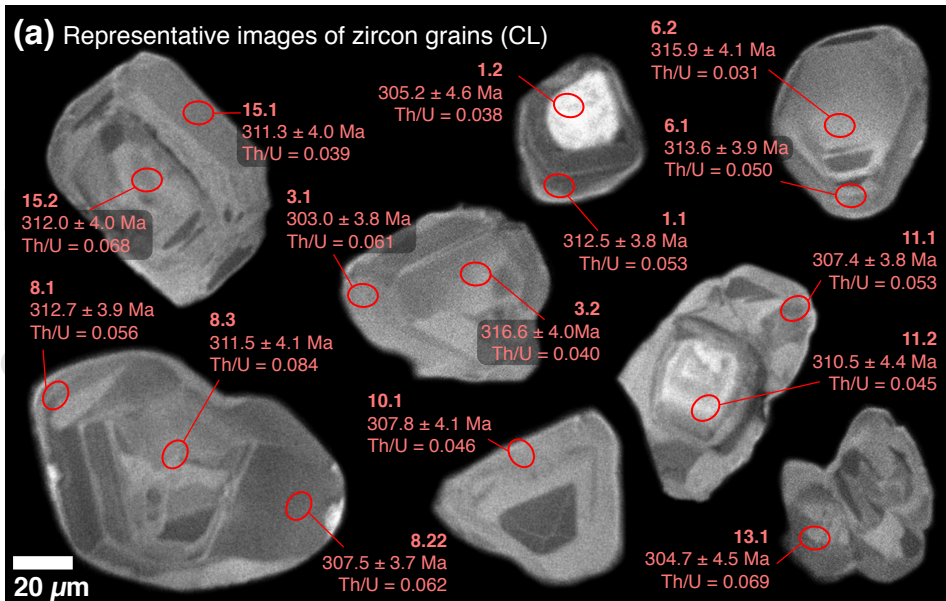
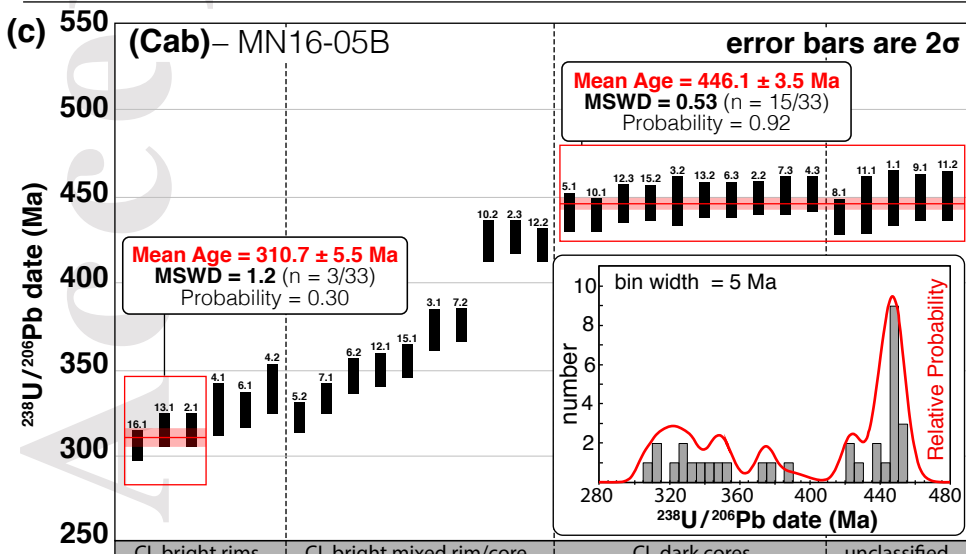
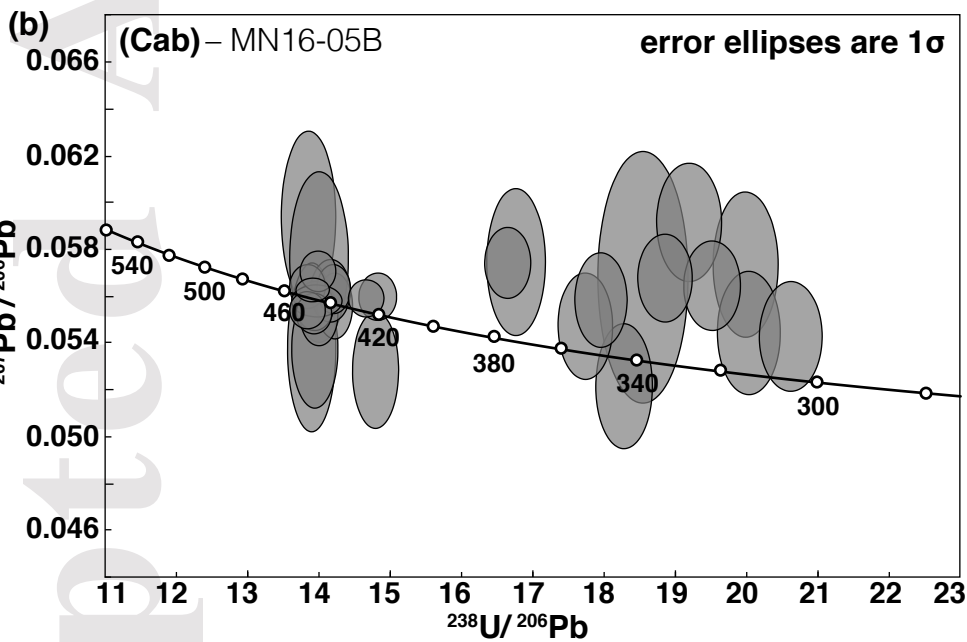
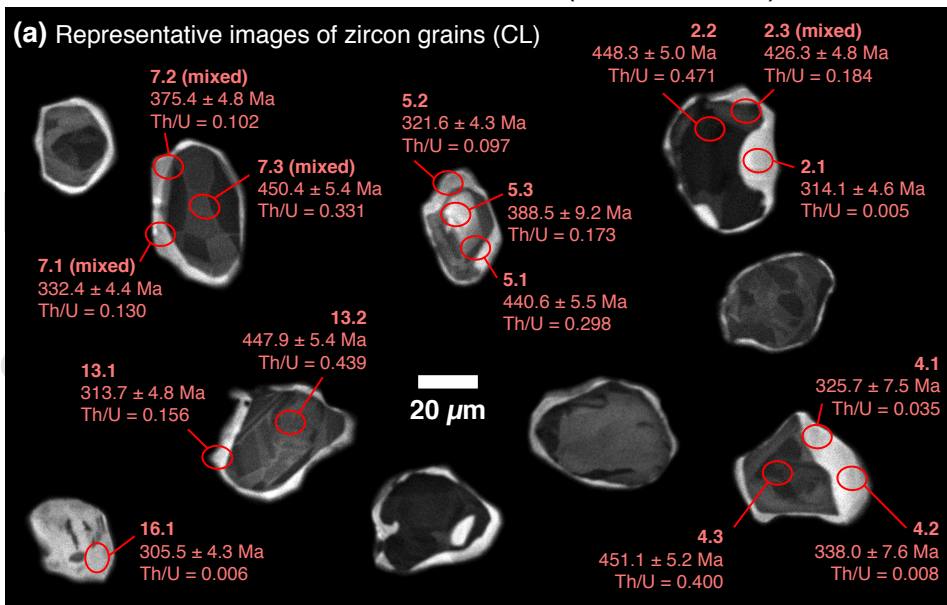


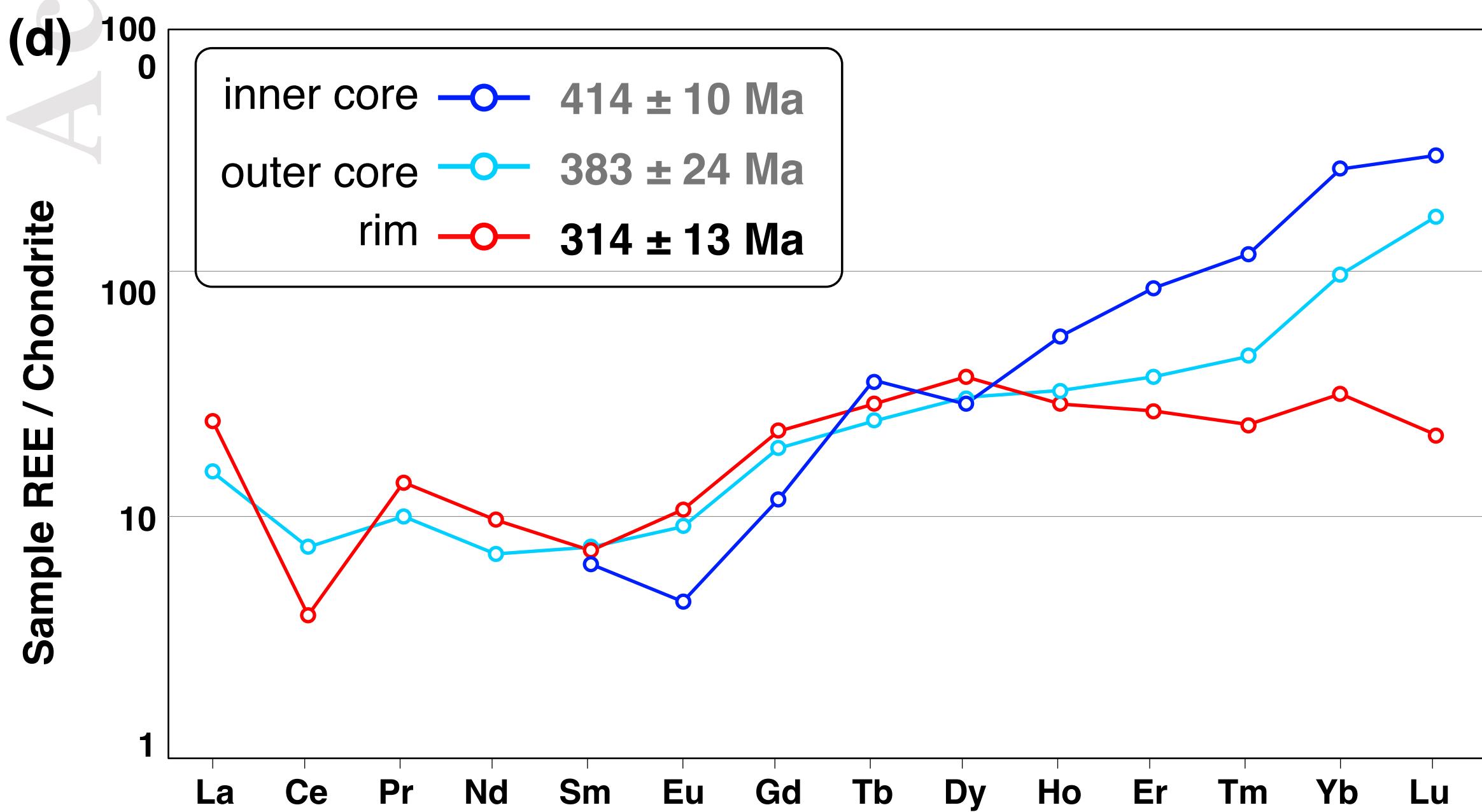
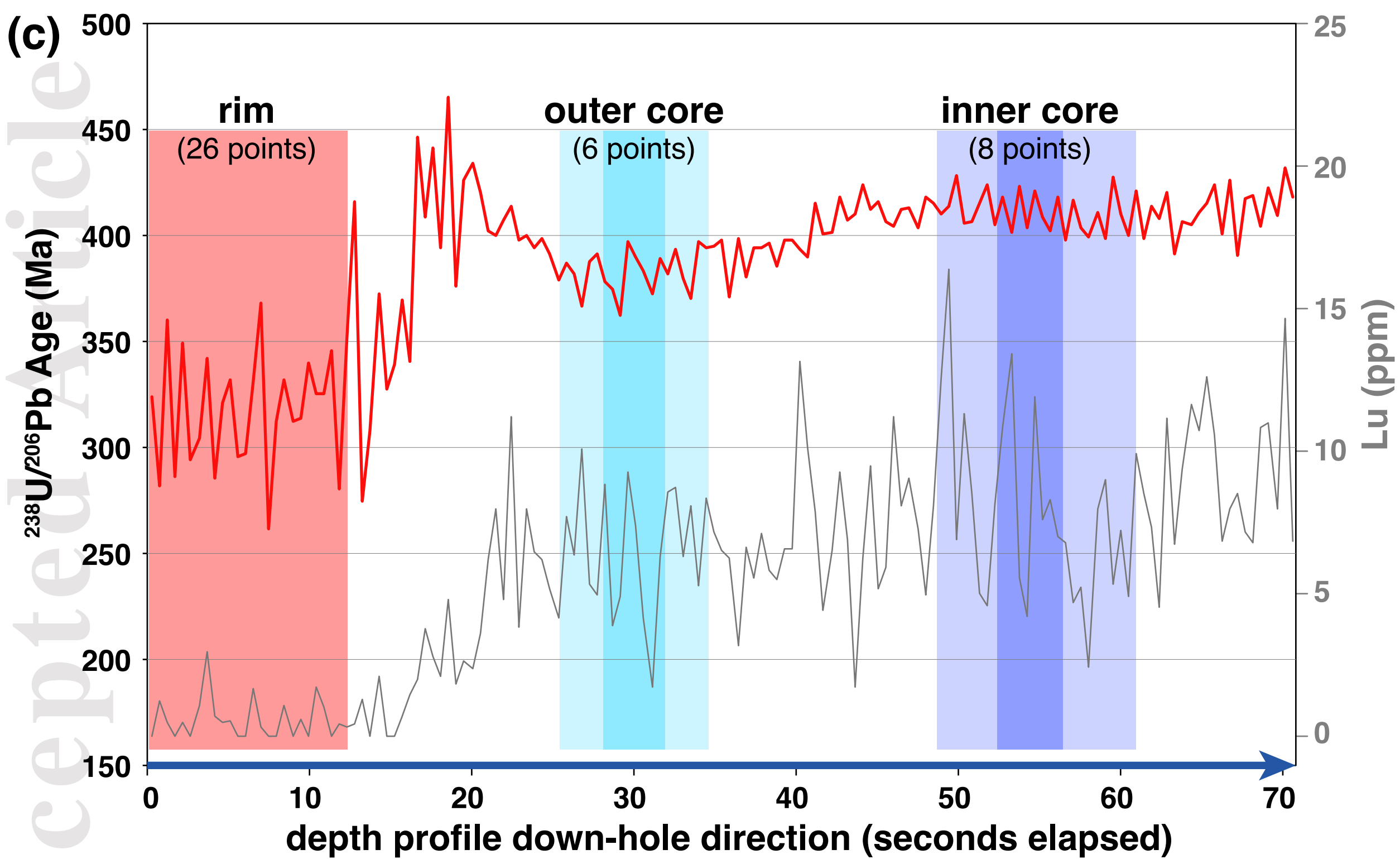
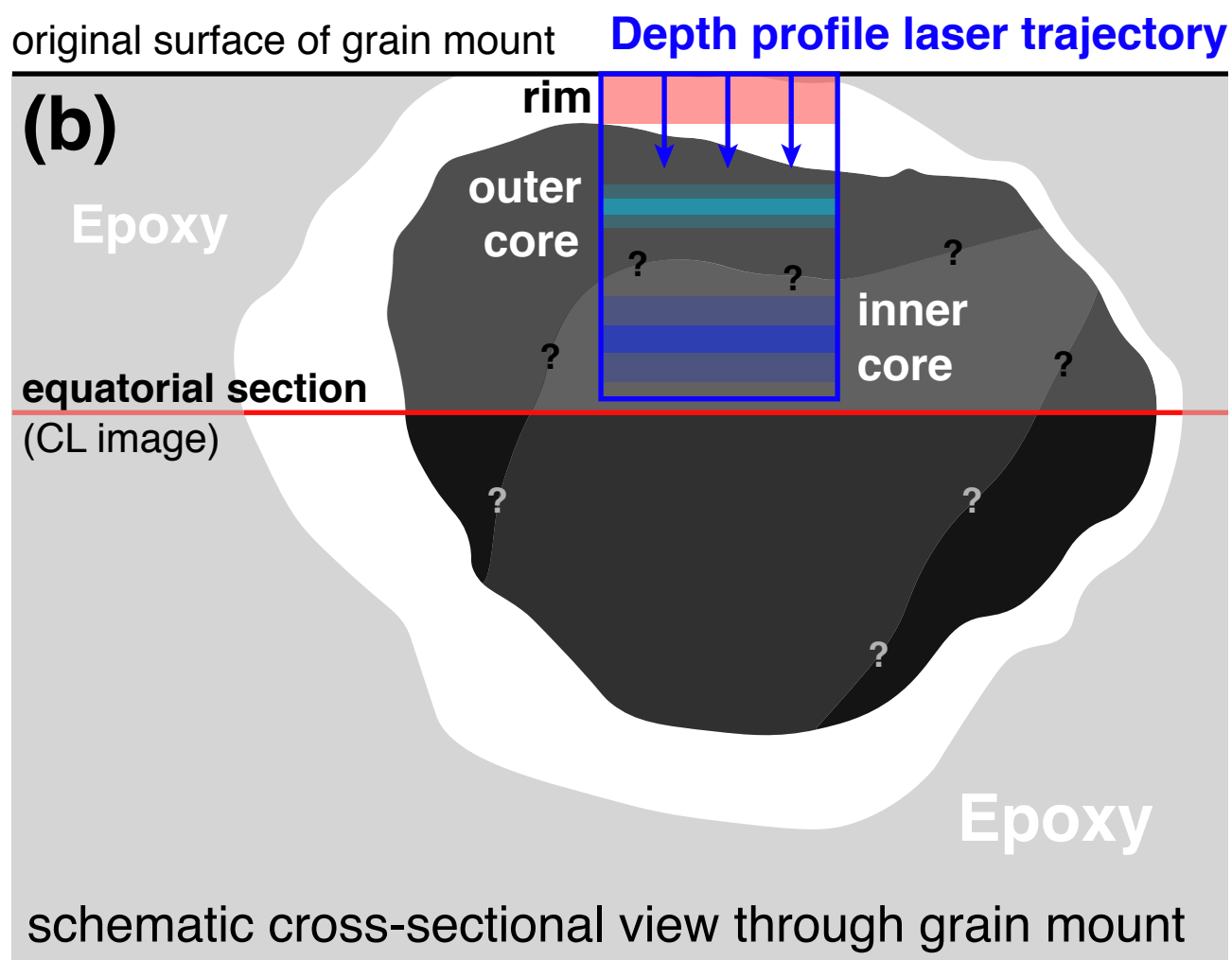
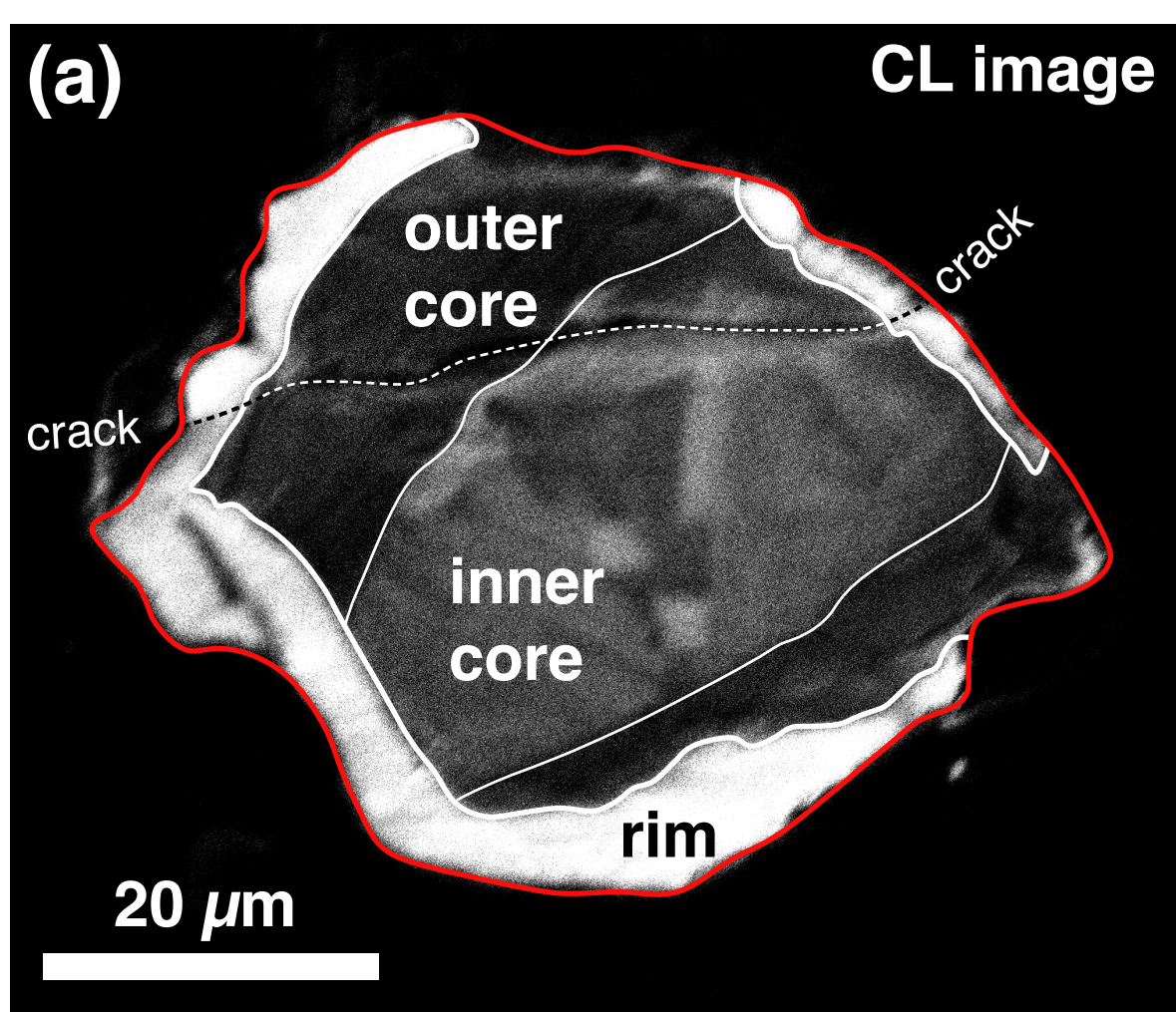
Figure 6

DOME CORE ECLOGITE (Terme de Fourcaric)

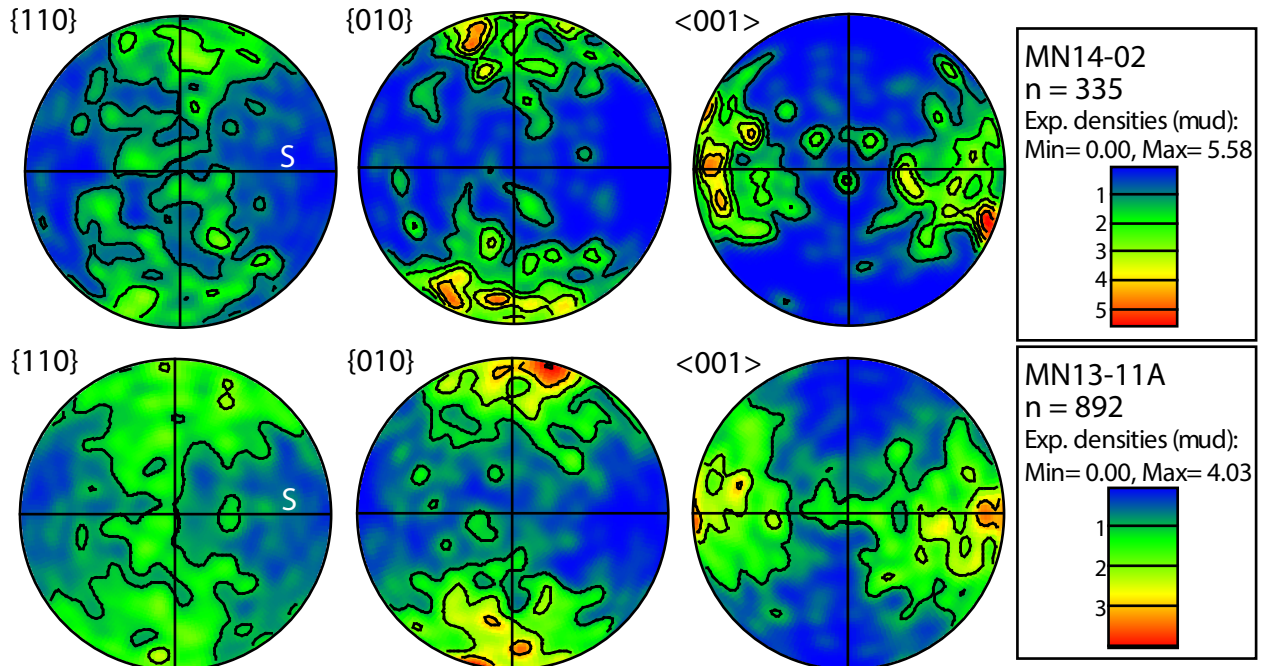


DOME-MARGIN ECLOGITE (Cabardès)





(a) dome-core eclogite (Terme de Fourcaric)



(b) dome-margin eclogite (Cabardès)

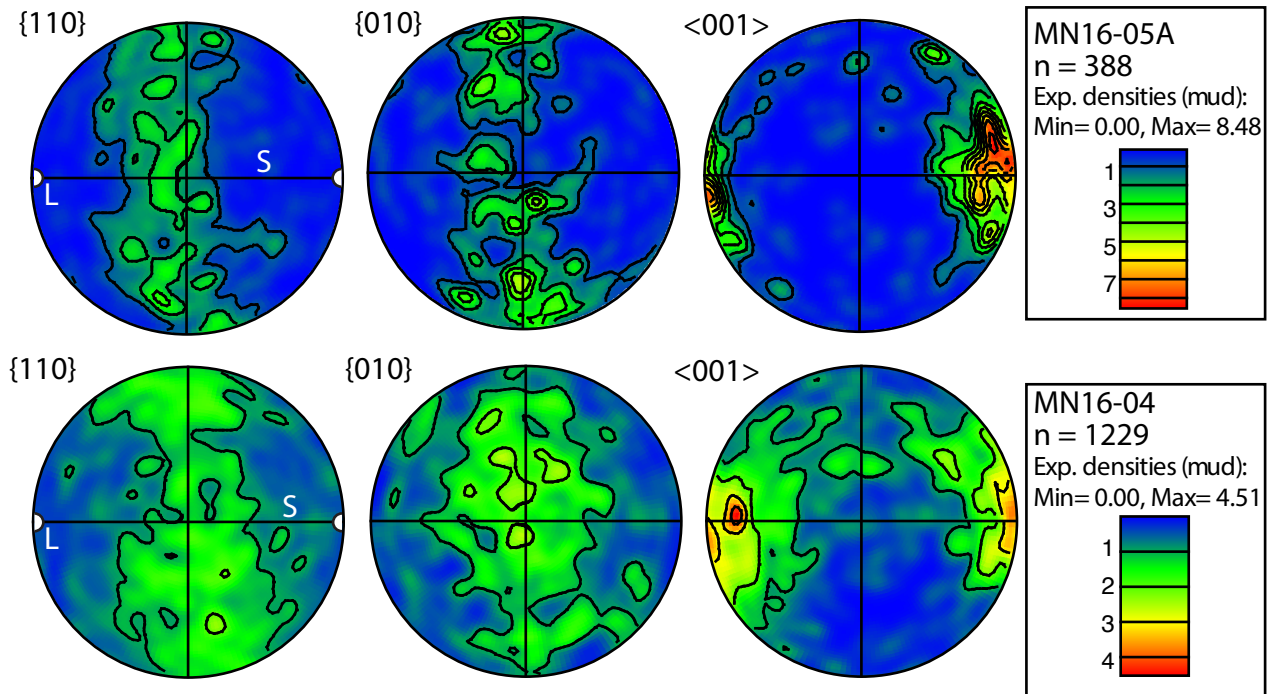


Figure 10

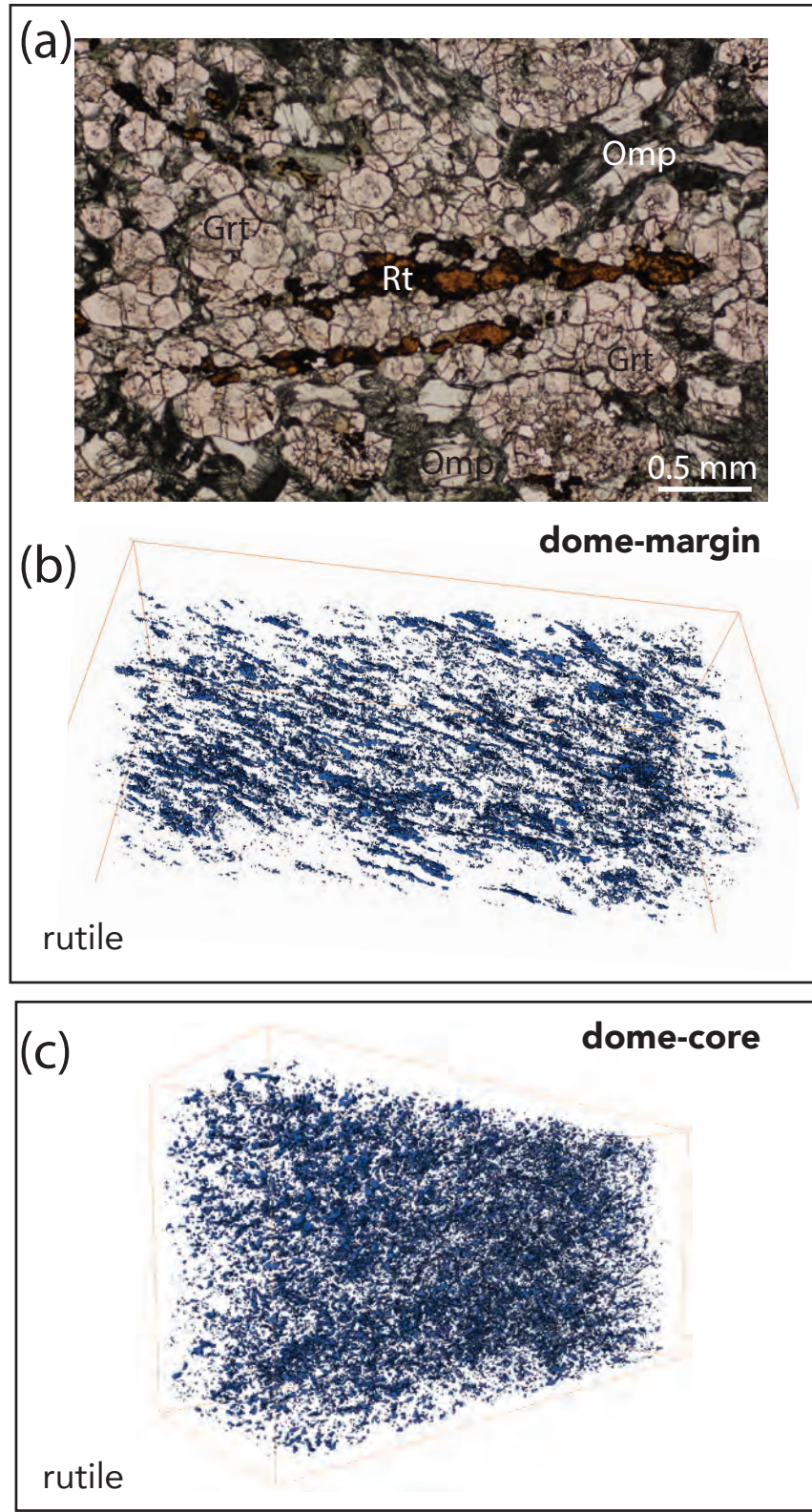


Figure 11

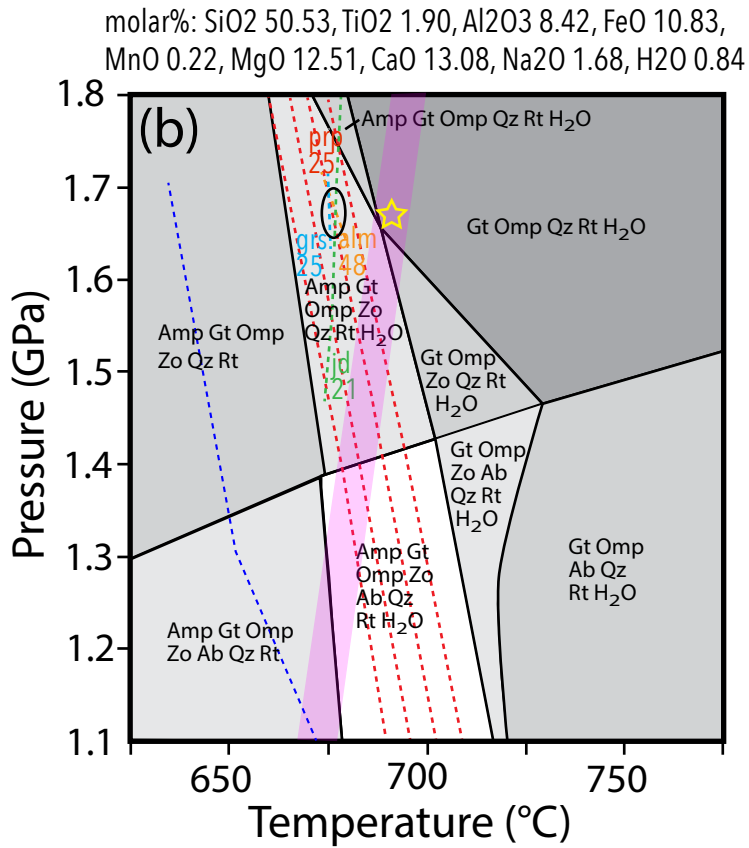
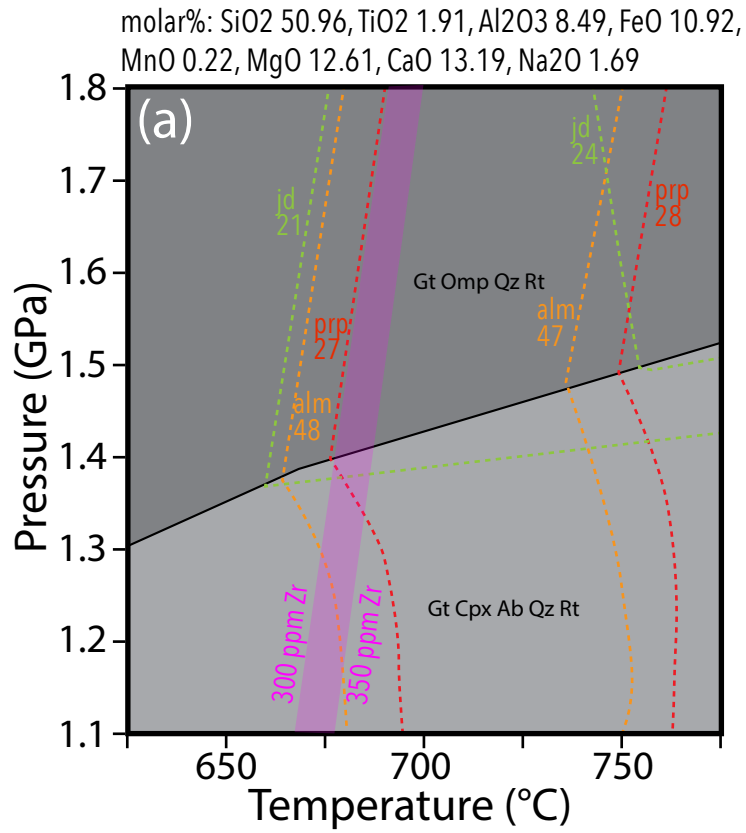


Figure 12

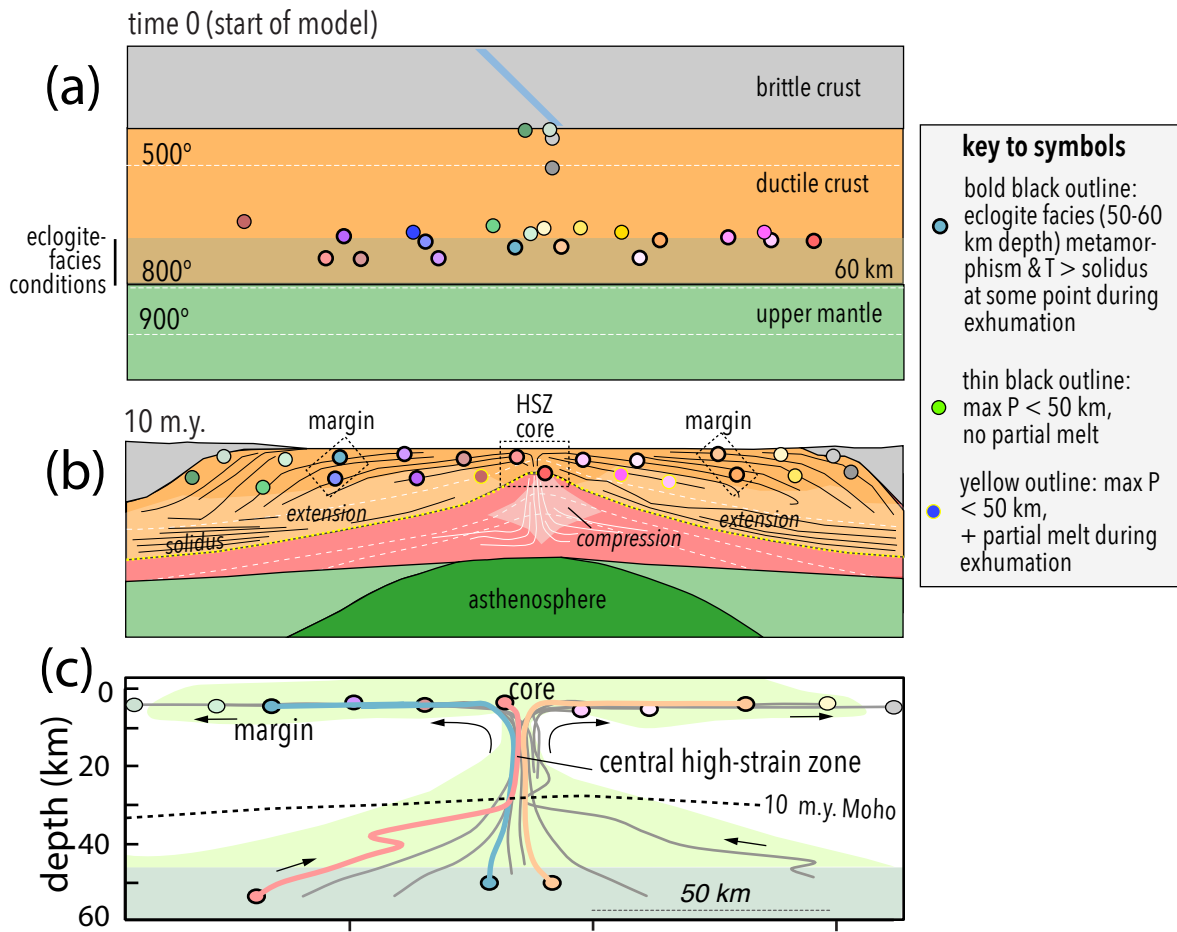


Figure 13

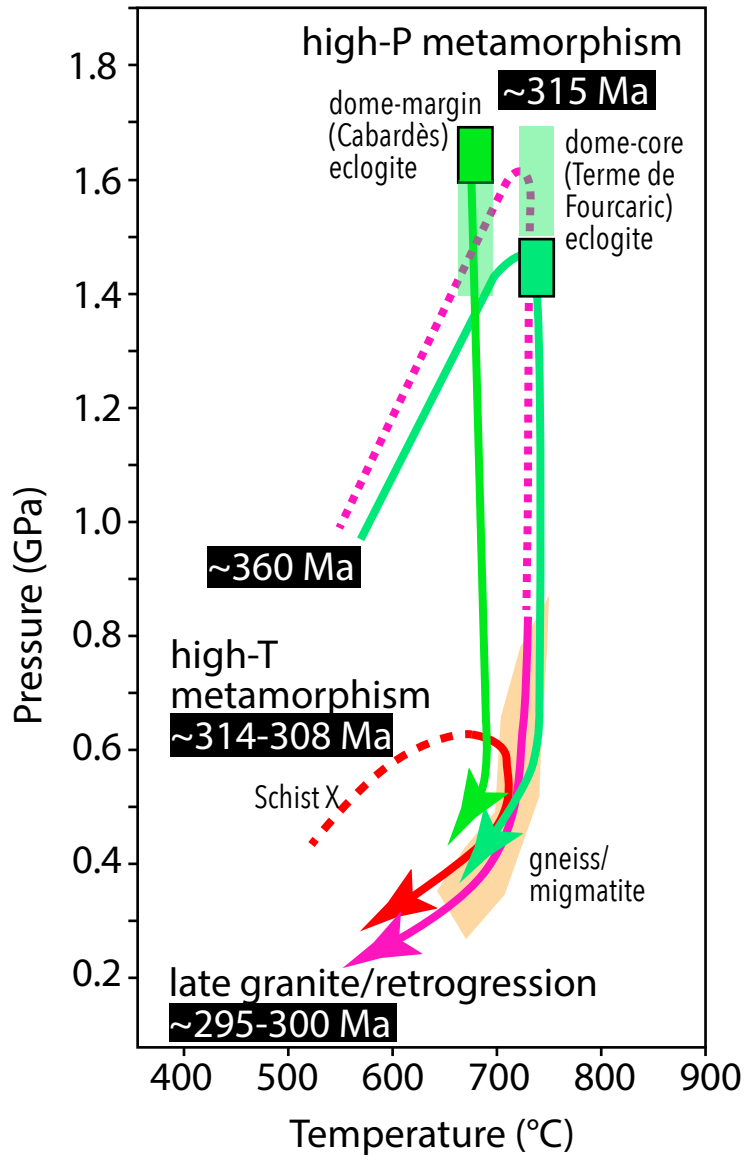


Figure 14